Chapter 2
Radiative Transfer Considerations

Know your lines and don't bump into the furniture.

—Spencer Tracy

Abstract In this chapter we describe some of the elements of radiative transfer that are necessary to understand the radiation coming from the diffuse interstellar medium. We concentrate on line processes. After a discussion of absorption and emission lines, we use the 21 cm line of hydrogen as an illustrative example. We also briefly discuss the CN transitions that are pumped by the Cosmic Microwave Background radiation. Collisional excitation, complications to radiative transfer from dynamical and nonlocal effects, and elemental abundances and depletions are also discussed. Molecular hydrogen and the Diffuse Interstellar Bands (DIBs) are used as examples of these effects. Finally, radio continuum processes are examined because they provide a way of measuring the properties of interstellar plasmas.

2.1 Introduction

Virtually everything we know about the interstellar medium derives from observing its effects on the passage of light.[1] Thus, it is important to understand how radiation is absorbed and emitted by gas and dust in the ISM as it propagates from its source to us. This comes under the broader subject of radiative transfer and it is covered in detail by many fine texts.[2] We assume in this section that the reader is familiar with the basics of radiative transfer and will limit ourselves to the more relevant and subtle aspects related to the diffuse ISM. We start with the radiative transfer equation as a general framework and concentrate on line transfer. After a discussion of absorption and emission lines, we use the 21 cm line of hydrogen as an illustrative example. We also briefly discuss the CN transitions that are pumped by the Cosmic Microwave Background (CMB) radiation. Collisional excitation, complications to radiative transfer from dynamical and nonlocal effects, and elemental abundances

[1] A part of the information also comes from studying cosmic rays but these are more indirect probes of the ISM.

[2] For instance, Chandrasekhar (1950), Cowley (1970), Athay (1972), Rybicki and Lightman (1979), Osterbrock and Ferland (2006), Hubeny and Mihalas (2014).

L. Magnani, S.N. Shore, *A Dirty Window*, Astrophysics and Space Science Library 442, DOI 10.1007/978-3-662-54350-4_2

and depletions are also discussed. Molecular hydrogen and the Diffuse Interstellar Bands (DIBs) are used as examples of some of these concepts. Finally, radio continuum processes are examined because they provide a way of measuring the properties of interstellar plasmas. The role of continuum processes in general for studying dust and the far infrared emission of the diffuse medium is postponed to Chap. 6.[3]

2.2 The Transfer of Radiation Through the Interstellar Medium

Radiative transfer theory describes how a beam of photons in a direction $\hat{k}$ of monochromatic intensity I_ν changes as it propagates through a medium. The beam can be extinguished by absorption (with coefficient κ_ν) and scattering (coefficient σ_ν) out of the line of sight, but photons can also be created by emission (with a coefficient j_ν) or injected by scattering *into* the line of sight. The intensity, having the units of a surface brightness (*cgs* units: ergs s^{-1} cm^{-2} $ster^{-1}$ Hz^{-1} or per unit wavelength in appropriate units, or Jy $sterad^{-1}$) is independent of distance and only changes along a line of sight by interactions. Calling the general monochromatic extinction coefficient κ_ν and the emission $j_\nu\rho$ (*cgs* units: ergs s^{-1} cm^{-3} $ster^{-1}$ Hz^{-1}), the simplest form of the equation of transfer is:

$$dI_\nu = -(\kappa_\nu I_\nu - j_\nu)\rho ds. \tag{2.1}$$

The *intrinsic* emissivity is independent of I_ν but any scattering terms depend on the *mean intensity*

$$J_\nu = \frac{1}{4\pi}\int I_\nu d\Omega \tag{2.2}$$

where Ω is the solid angle. The scattering includes the angular distribution of the photons coming from some direction $\mathbf{k}'$ and scattered into the direction $\mathbf{k}$ through the coefficient α:

$$\text{(scattering term)} = \frac{1}{4\pi}\int \alpha(\hat{k}', \hat{k})\sigma_\nu I(\hat{k}')d\Omega'. \tag{2.3}$$

When diffuse radiation is important, scattered light can change level populations depending on the background spectrum. This is important for the far infrared, in the

[3] A word of warning to the reader. In this chapter, because of the broad range of applications found in line formation theory to atoms and molecules, we will treat them on the same footing. Sometimes, we will switch between them in a single discussion but we hope the context will make clear what we are referring to.

densest clouds, and certainly in stellar atmospheres and even HII regions, but it can be safely neglected in the diffuse ISM. Scattered light is especially significant when treating dust but also a primary mechanism for making dark lines. The radiative energy density is related to the mean intensity by

$$\epsilon = \frac{1}{4\pi c} \int \int I_\nu d\Omega d\nu. \tag{2.4}$$

Since the *point spread function* (*psf*) of any telescope is finite, the source is always observationally convolved with the beam. However, intensity is not measured if the source is smaller than the beam. For these what is routinely measured is actually the monochromatic *flux* (also called the flux density), the intensity integrated over the solid angle of the *psf* or its decomposition of flux density per beam in the direction relative to the surface normal:

$$F_\nu = \int_{beam} I_\nu(\hat{k}) \hat{\mathbf{k}}' \cdot \hat{\mathbf{n}} d\Omega \; / \int d\Omega \tag{2.5}$$

where $\mathbf{n}$ or $\hat{\boldsymbol{n}}$ is the surface normal relative to the line of sight and the integral is over the *psf* or beam of the telescope.

A photon can disappear either altogether or simply deviate from the direction of the observer. The former is a true absorption event and, as we will see, couples the radiation directly to the gas. The latter conserves photon number if it is coherent, or redistributes the energy among several emergent photons. The distinction is important. In a sufficiently dense medium, the incident photons are destroyed by collisions and the energy is redistributed within the "thermal pool" of the ambient particles that are not the absorbers. In such case, the excitation of the ions is governed by the energy distribution of the colliding particles. Instead, if the collisions are relatively rare, as in the diffuse ISM, the absorption event ends in a radiative de-excitation, the decay of the excited state, and the populations are determined by the spectrum of the incident photons. The same is true of the emergent spectrum. The ratio of the emissivity to absorption is called the *source function*

$$S_\nu = \frac{j_\nu}{\kappa_\nu} \tag{2.6}$$

which, for thermal equilibrium, is the Planck function, $B_\nu(T)$, at temperature T.

The optical depth of the medium is a measure of the extinction and is defined[4]

$$d\tau_\nu = -(\kappa_\nu + \sigma_\nu)\rho ds. \tag{2.7}$$

[4]The choice is to use the absorption coefficient per unit mass, which requires the mass density ρ, or per absorber, so one uses the number density n. Only consistency is needed, the two are formally the same.

In the absence of internal sources, the solution to equation 2.1 for an incident intensity $I_\nu(0)$ is:

$$I_\nu = I_\nu(0)e^{-\tau_\nu}. \tag{2.8}$$

This result differs from the usual presentation in discussion of stellar atmospheres since we are treating a single line of sight toward a point source rather than specifying a geometry for the intervening medium and treating diffuse radiation.

Although simple, equation 2.8 is actually profound. Re-interpreted, it gives that the probability (ignoring emission by the medium) of a photon at any frequency penetrating a scaled distance τ_ν in a medium in any direction. The photon's probability of emerging from a medium if its source function is uniform is a Poisson process (individual photons with an exponential distribution in penetration)

$$I_\nu = S_\nu(1 - e^{-\tau_\nu}). \tag{2.9}$$

The optical depth is the measure for a gas of its transparency to photons. and should *not* be confused with a probability of transmission. More importantly, it is an integrated quantity along the line of sight and cannot distinguish individual contributors. In the same way that independent probabilities multiply, the optical depths simply add at a fixed frequency. Therefore, if we have individual clouds along a line of sight, each contributes separately depending on the frequency.

2.2.1 Statistical Balance

We can now derive the emission and absorption coefficients. The level populations are determined by the competition between radiative and collisional rates. These form the link between the phenomenological measures and the microphysical properties. Since in this chapter we will usually deal with resonance transitions, we will use a two level system as our paradigm. The two levels are $E_i = 0$ and $E_j > E_i$. The governing equation, neglecting ionizations, is given by local statistical equilibrium, linking all radiative and collisional processes. The *steady state* rate equation for this two-level system links the level populations n_i and n_j to the ambient radiation J_ν and electron density n_e:

$$(n_j B_{ji}\Phi_{\nu,em} - n_i B_{ij}\Phi_{\nu,abs})J_\nu + (n_j C_{ji} - n_i C_{ij})n_e + (n_j A_{ji}\Phi_{\nu,em}) = 0 \tag{2.10}$$

where we have grouped together the stimulated absorption and emission terms that depend on the arrival rate for photons of frequency $\nu = (E_j - E_i)/h$ in the first parentheses, the collisional terms in the second, and the spontaneous decay from the upper level in the third. The rates for the radiative processes are the Einstein

A and B transition probabilities, and $\Phi_{\nu,abs}$ and $\Phi_{\nu,em}$ are the profile functions for absorption and emission, respectively. The collision rates are C_{ij} and C_{ji} where

$$C_{ij} = \int_{\Delta E}^{\infty} \sigma_{ij}(E)\ v f(E) dE. \tag{2.11}$$

In this equation $\sigma_{ij}(E)$ is the energy dependent collision cross section, v is the relative velocity, and $f(E)$ is the energy distribution of ambient electrons (not necessarily a Maxwellian).[5] The downward rate has no threshold, so $\Delta E = 0$, while for the excitation rate the lower limit on the integral is $\Delta E = E_j$. If collisions are sufficiently frequent that they balance separately from radiative rates, the level populations are fixed by the kinetic temperature of the electrons, T_{kin}. The radiation is then in thermal equilibrium with matter, this condition is called *local thermodynamic equilibrium* (LTE) because it is valid on the microscopic scale set by the collisional mean free path and $T = T_{kin}$. The level populations are governed by collisions separately from the radiative processes in what is called *detailed balance*. If the emission and absorption profiles are the same, an assumption called *complete redistribution*, then the ratio of the radiative terms determines the energy distribution of the radiation

$$J_\nu = A_{ji} n_j / [n_i B_{ij} - n_j B_{ji}]. \tag{2.12}$$

This is the source function we defined earlier, the ratio of the emission to absorption coefficients. For LTE, J_ν is the Planck function

$$B_\nu(T) = \frac{2h\nu^3}{c^2} \frac{1}{e^{h\nu/kT} - 1} \tag{2.13}$$

and level populations follow a Boltzmann distribution

$$\frac{n_j}{n_i} = \frac{g_j}{g_i} e^{-h\nu/kT} \tag{2.14}$$

where the statistical weights of the two levels are (g_i, g_j). Substituting equation 2.14 into 2.12 provides the *definition* of the Einstein transition probabilities:

$$A_{ji} = \frac{2h\nu^3}{c^2} B_{ji}, \qquad g_i B_{ij} = g_j B_{ji}. \tag{2.15}$$

The emission is then given by

$$j_\nu = h\nu A_{ji} \Phi_\nu n_j \tag{2.16}$$

[5]Note that the perturbers can also be H atoms and H_2 molecules, or even He atoms. The electrons will be the most important, mainly because of their mass, and they have much larger mean velocities than the protons. But the same formalism applies to molecules and atoms.

and the absorption coefficient is

$$n_i \kappa_\nu = n_i B_{ij} \Phi_\nu (1 - e^{-h\nu/kT}); \tag{2.17}$$

where the exponential accounts for the stimulated emission rate.

2.2.2 Radiative Processes in the Rayleigh-Jeans Limit

We are going to deal extensively with molecules and long wavelength observations so we will often be in the regime $h\nu_0 \ll kT$. This is the called the Rayleigh-Jeans limit for the Planck function implying LTE. The solution for the transfer equation then becomes

$$T_B = (T_{ex} - T_{bg})(1 - e^{-\tau_\nu}). \tag{2.18}$$

Here, T_B is the brightness temperature of the emitting gas, defined as $T_B = I_\nu c^2 / 2k\nu^2$—see Sect. 4.2.6), T_{ex} is the excitation temperature of the medium, and T_{bg} is the brightness temperature of a background beyond the medium. Properly speaking, T_B is really ΔT_B, the difference in a radio measurement towards a source and off the source. We will discuss *on/off observations* as these types of measurements are called by radio astronomers in Sect. 4.2.2. When $\tau \gg 1$, equation 2.18 becomes $\Delta T_B = T_{ex} - T_{bg}$ and observations of T_B provide information on the excitation temperature of the medium. In the optically thin case, when $\tau \ll 1$, equation 2.18 reduces to

$$\Delta T_B = (T_{ex} - T_{bg})\tau_\nu. \tag{2.19}$$

Most molecular transitions in the diffuse ISM are optically thin so that this equation may be used together with an expression for the absorption coefficient, κ_ν to derive the column density of the ionic species in question.[6] We show how this is done in Sect. 2.2.5 .

2.2.3 The Line Profile Function

The line emission and absorption coefficients require knowing the intrinsic profile for the transition. This is a Lorentzian function that has the same form as a damped

[6]Ironically, the principal transition for tracing molecular gas in the ISM, the CO(1-0) line at 115 GHz or 2.6 mm, is often optically thick even in the diffuse ISM.

harmonic oscillator.[7] For the classical emission mechanism, a radiation damped harmonic oscillator (e.g. Jackson 1999), the classical damping rate is

$$\Gamma_{rad} = \frac{2}{3}\frac{e^2\nu_0^2}{4\pi^2 m_e c^3}. \tag{2.20}$$

This, however, is modified by the quantum mechanical selection rules depending on the multipolarity of the transition. This Γ_{rad} now includes the *oscillator strength*, f_{ij},

$$\frac{\pi e^2}{mc} f_{ij} = \frac{h\nu}{4\pi} B_{ij}. \tag{2.21}$$

The generalized Γ_{rad} value depends on the transition probabilities (the equivalent of a Q-value for an oscillator)—the lifetimes of the levels i and j together. However, most of the observable absorption lines from the diffuse ISM are from the ground state so the broadening is due to the excited state so that $\Gamma_{rad} = \Gamma_{ij} = A_{ji}/4\pi$ and the absorption coefficient is

$$\kappa_\nu = \frac{\pi e^2}{mc} f_{ij} \frac{\Gamma_{ij}}{4\pi} \frac{1}{\Delta\nu^2 + (\Gamma_{ij}/4\pi)^2}. \tag{2.22}$$

The line optical depth is proportional to $g_i f_{ij}$.

Besides the intrinsic profile, each atom also has a random thermal motion that Doppler shifts the frequency of any absorbed or emitted photon. Hence, although the rest frequency is precisely defined, the ensemble of particles has a three dimensional Gaussian velocity distribution relative to the photons. In an absorbing medium, the effect is only along the line of sight so the chance that a photon will be seen at any frequency $\Delta\nu$ relative to ν_0 is

$$G(\Delta\nu) = (2\pi\Delta\nu_D^2)^{-1/2} e^{-(\Delta\nu/\Delta\nu_D)^2} \tag{2.23}$$

where

$$\Delta\nu_D = \frac{\nu_0}{c}\left(\frac{2kT}{Am_p}\right)^{1/2} \tag{2.24}$$

is the *thermal* Doppler width of the line for a species of atomic mass A. For the diffuse ISM it would be around $0.1(T/10\ K)^{1/2}A^{-1/2}$ km s^{-1}. However, observed line widths are often much larger than this, up to several km s^{-1}, and independent of the atomic mass. So nonthermal motions are clearly important. If such dynamical broadening is due only to uncorrelated motions, with a typical random speed σ, the

[7] See, e.g., Griem (1964, 1997), Spitzer (1978), Rybicki and Lightman (1979), Draine (2011), and Hubeny and Mihalas (2014).

thermal and dynamical contributions add in quadrature, $\Delta\nu_D^2 = \Delta\nu_{D,th}^2 + (\nu_0\sigma/c)^2$. Regardless of the microphysical intrinsic profile, the random motions broaden the line at each $\Delta\nu$ and the total profile is the convolution $P(\nu) = G \star \Phi$. For an intrinsic Lorentzian profile, the convolution function is the so-called Voigt profile

$$H(v,a) = \frac{a}{\pi^{1/2}} \int_{-\infty}^{\infty} \frac{e^{-x^2} dx}{(v-x)^2 + a^2} \tag{2.25}$$

where $a = \Gamma/(4\pi\Delta\nu_D)^{1/2}$ is the dimensionless line width and the integration variable (whether in wavelength or frequency) is normalized to the Doppler width. If a is very small (for a Gaussian much broader than the Lorentzian for any reason), the Voigt profile is like a convolution of a Gaussian and a δ-function so the resulting profile is also Gaussian. For each species, the full width half maximum is given by $2.35\nu_0\sigma/c$ and if T is constant along the line of sight, the FWHM of lines of different atoms depends only on the atomic weight. If, on the other hand, the thermal broadening is negligible compared to the intrinsic line width, the profile will be Lorentzian. For such a profile, the FWHM is defined but the dispersion (second moment) is not and the wings will be much broader than for a Gaussian. For large $\Delta\nu$, the profile varies as $\Delta\nu^{-2}$ (see Fig. 2.1).

Only an uncorrelated random velocity field will produce a Gaussian profile. This is sometimes referred to as *macroturbulence*, although the term is a misnomer. The hypothesis is that whatever the magnitude of the velocities, they are distributed in a sort of fully developed (homogeneous, isotropic) chaos. So being independent of the thermal motions, this macroscale contributes another Gaussian with a dispersion σ that depends on the larger scale random motions and *not* on the thermal width, σ_T.

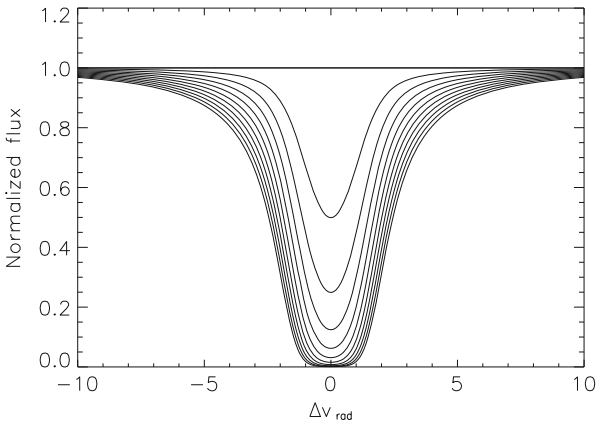

Fig. 2.1 Variation in the absorption (in normalized flux units) as a function of radial velocity (in scaled units) for a series of Voigt profiles with equivalent widths in scaled units from 0 to 1000 in steps of 10% starting from zero (so 0,100,200,...,1000). Note the increase in the wings once the profile saturates at line center

Since the convolution of two Gaussian profiles is another Gaussian with the width being given by $(\sigma^2 + \sigma_T^2)^{1/2}$, the relative contribution of the Lorentzian wings to the line profile is reduced. Macroscopic motions may not be drawn from a normal distribution but they shift the frequency of the transition from ν_0 along the line of sight. This is where the ISM is very different from a stellar or planetary atmosphere. Since the medium is *not* in hydrostatic equilibrium, there are virtually no constraints on the velocity field. Not only can the motions be supersonic but the line of sight can pass through regions that have nothing mechanically to do with each other. We will return to this in more detail when discussing observations of turbulence in Chap. 11, but for now we simply ask what macroscopic motions do to the line formation.

In denser plasmas, collisions significantly reduce the lifetime of excited states and broaden the levels. In general, this is not important under interstellar conditions. Yet collisions cannot be completely ignored. In the absence of a strong radiation field, excitation can still occur if the energy differences are of the same order or less than the thermal energy. For instance, consider the CO(1-0) transition, the lowest rotational line at 115 GHz for the $^{12}C^{16}O$ isotopic composition. For cold environments, in the absence of a background source of radiation, the excitation is governed by collisions followed by radiative de-excitation. Therefore the strength of the line depends on the collision rate, hence on the thermal pool of the gas. While this is not really in LTE, the excitation temperature, hence the brightness temperature, is close to the kinetic temperature of the colliding H_2 molecules that are principally responsible for the excitation in the molecular medium. Every emitted photon, corresponds to a collision no matter how low density the medium may be so the luminosity depends on the CO/H_2 ratio. This is the origin of the so-called "CO to H_2 conversion factor", conventionally designated as X_{CO} (this conversion factor is discussed extensively in Chap. 8). The masses of the emitting region are thus determined by a proxy measure based on the line that can be *observed* while the H_2 is virtually invisible in wavelengths longer than the far ultraviolet (FUV) where the electronic state absorptions are detectable (in contrast to the atomic case, aside from the UV there is no strong background against which the lines can absorb and the transition probabilities are relatively low).

The lack of collisional de-excitation greatly simplifies the treatment of *absorption* line formation. Furthermore, for atomic resonance line absorption, collisional excitation plays no role, so the only temperature dependence of the column density comes from the ionization fraction.[8] For the transfer equation, large scale velocity fields (i.e. shear flows or ordered motions that have large velocity gradients), turbulence, and thermal Dopper broadening all combine to desaturate a line profile. The overall transparency of the gas at any frequency increases and, for the curve of growth (see the next section), this extends the range of column density over which the absorbed fraction of light along the line of sight is linearly proportional to the optical depth at line center and $\tau \sim N$. The normalization is over a broader profile

[8]The only complication arises when treating fine structure lines, such as [CII] at 158 μm, because collisions affect the population ratios for the atomic levels.

so the column density required to produce the same equivalent width increases. This also delays the onset of the saturated portion of the curve of growth and the column density at which the Lorentzian wings contribute to the total absorption.

It should be emphasized that *any* macroscopic motions, provided that they exceed the thermal broadening, will produce a similar effect. The difference between different mechanisms is in the detailed change in the profile. For instance, an ordered magnetic field also desaturates the profile since it decreases the optical depth at line center by redistributing the absorption over the Zeeman components. The profile is not, however, Gaussian so the change in the curve of growth with column density will not be the same as desaturation of a purely random field. This is true even though each component in the split line is thermally broadened (and also macroscopically affected). The one important difference is that since the Zeeman effect is coherent for an ordered field there is no coupling between the states and the profile can be distinguished by polarization. This is important for Zeeman measurements, for instance using the 21 cm line, since the magnetic fields are usually very weak in the ISM. For *integrated, unpolarized* measurements, it is possible that the random motions dominate and the profile looks Gaussian.

The effect of a magnetic field on line profiles is rather simply treated for interstellar lines of sight since the individual lines are formed under collisionless conditions. Observationally, however, measuring the field strengths is very challenging. The splitting of optical lines is far too small for any measurements of the splitting since the fields are of order μG. but since the separation of components varies as λ^2, radio observations can measure the fields. Direct measurements of Zeeman splitting in integrated profiles is exceedingly difficult since a field of microGauss, typical of the diffuse phase, produces a negligible splitting relative to the dynamical and thermal broadening of the profiles (of order 1.4 Hz μG^{-1}; e.g., Fig. 4.5). However, using circular polarization, the degree of polarization measured from the difference in intensity between two circular polarization states, is directly proportional to the field strength (see the recent review article by Crutcher 2012). These measurements are unaffected by self-absorption or other optical depth effects so the only requirement is sufficient signal to noise ratio to obtain the field. Successful measurements of the Zeeman splitting of low-lying CN transitions ($N = 2 - 1,\ N = 1 - 0$) have been achieved in dense clouds (e.g. Crutcher 2012, 2014). The competition between collisional coupling and radiative transitions in the presence of velocity shears (large scale flows) can enhance the polarization by changes in the optical depths of the Zeeman components but this has not been seen, yet, in low density clouds (Goldreich and Kylafis 1981). It is another case in which the escape probability formalism with flows makes the treatment of the radiative level couplings simpler.

2.2.4 *Obtaining Column Densities from Absorption Lines: Equivalent Width and Curve of Growth Methods*

The discovery of the diffuse interstellar medium was a *spectroscopic* accident. Observations of the radial velocity variations of several unresolved binary stars, especially δ Ori, led Hartmann in 1904 to identify stationary absorption lines with the presence of unbound gas interposed between the stellar system and the Earth. The centroid velocities of these features was neither that of the center of mass of the binary nor directly related to any of the neighboring stars. They were also specific, two absorption lines that were normally not seen in the spectrum of the hot stars being studied. The two main optical atomic absorption features are the doublets of NaI 5889, 5895 Å and CaII 3933, 3968 Å. Importantly, both are resonance lines of their respective ions and both are doublets. The NaI D lines, $2p^6 3s^2 S_{1/2} - 2p^6 3p^2 P^o_{3/2,1/2}$ share a common lower state and CaII H and K, similarly, have almost identical behavior, $3p^6 4s^2 S_{1/2} - 3p^6 4p^2 P^o_{3/2,1/2}$ with the higher J value being the upper state. Because of the difference in statistical weights of the multiplet substates, the components differ by almost 0.3 in log gf and therefore have different optical depths at any column density.

The most important property of absorption lines arising from the diffuse interstellar medium is that they are seen in absorption *against* something external. This is not as circular a statement as it might seem. A stellar or extragalactic, continuum source (or even line emitter) has no interaction with the intervening medium. Yet, unlike the effect of an optically thickness on the emission lines formed within a cloud, the ability to see the illuminating object implies that one sees completely through the absorbing medium. If the distance to the background source is known, this provides an unambiguous measure of the mean volume density within the resolution of the spectrum. Low density clouds have such low optical depths, however, that the highest velocity portions of the profile can frequently be missed.

To quantify the total (absorption plus scattering) extinction fraction of the light removed by dark lines from any portion of the spectrum, a convenient measure is the *equivalent width*, W_λ, defined by

$$W_\lambda \equiv \int_{-\infty}^{\infty} \Big(1 - \frac{I(\Delta\lambda)}{I(\lambda_0)}\Big) d\Delta\lambda \tag{2.26}$$

where λ_0 is the wavelength at line center. The integral is taken over the entire profile (or any band of the spectrum). Since the units are usually Ångstroms, the integral is written in wavelength units and the unit of W is Å although this choice of dimensions is purely conventional. Note that since the intensities are normalized to the continuum, W_λ is independent of distance. What is seen from the definition is that W_λ has several important limits depending on the line profile. Writing $\tau_\nu = \tau_0 \Phi_\nu$ where $\Phi(\Delta\lambda)$ is the (normalized) line profile function and τ_0 is the

optical depth at line center,

$$W_\lambda = \int_{-\infty}^{\infty} (1 - e^{-\tau_0 \Phi(\Delta\lambda)}) d\Delta\lambda . \tag{2.27}$$

Even without precisely connecting the opacity with a specific transition, in the limit of a nearly transparent medium—when τ_0 is very much smaller than unity—the equivalent width varies as

$$W_\lambda \sim \tau_0 \sim N_i \tag{2.28}$$

since τ_0 is proportional to the column density of the lower state N_i. For a Gaussian line profile with full width at half maximum (FWHM), $\Delta\nu$,

$$\tau_i = \left(\frac{ln\,2}{\pi}\right)^{1/2} \left(\frac{2}{\Delta\nu}\right) \frac{\lambda^2}{8\pi} A_{ji}\, \frac{g_j}{g_i}\, N_i \left[1 - exp\left(-\frac{h\nu}{kT_{ex}}\right)\right], \tag{2.29}$$

and the column density for a weak line scales as

$$N_i = 1.1 \times 10^{20} \lambda^2 f_{ij}^{-1} W_\lambda(\text{Å})\, \text{cm}^{-2}. \tag{2.30}$$

Here λ is in Å. With increasing optical depth the residual intensity at line center approaches zero but, because the profile is not a δ-function, there is always additional absorption from beyond line core, depending on the form of Φ. This is the *saturated* rate of growth of the profile, when the equivalent width increases more slowly than linearly with increasing column density. For a Lorentzian dominated line, also called a *damped absorption line* (as in the cosmological case of the Ly α forest), the curve of growth yields $W_\lambda \sim N_i^{1/2}$, as seen from Fig. 2.2. The effect of gf on the line strength is shown in Fig. 2.3.

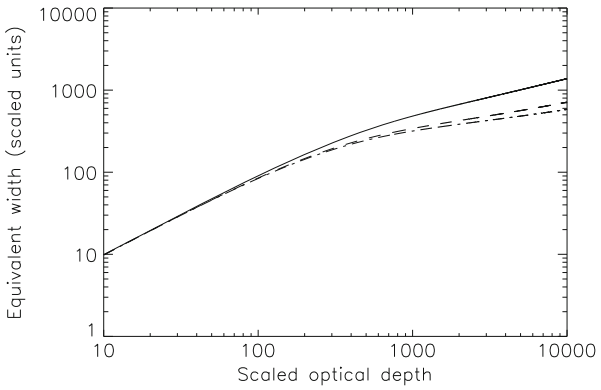

Fig. 2.2 Sample curve of growths in scaled units for a= 0.5 (*solid line*), 0.1 (*dashed line*), and 0.05 (*dash-dot line*)

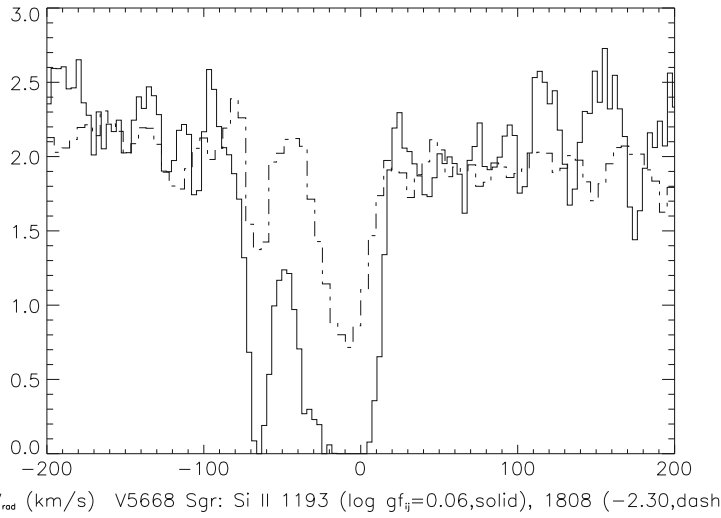

Fig. 2.3 Absorption lines along the line of sight to the nova V5668 Sgr 2015. The *solid line* is Si II at 1193 Å and the *dot-dashed line* is the 1808 Å line. This figure illustrates the effects of log (gf)

The lower level of an observed transition need not necessarily be the ground state, even under interstellar conditions. Fine structure states, because of their very small separations, can be collisionally excited even in the warm medium. Notwithstanding that such events are extremely rare, the induced populations may suffice to produce detectable absorption. Thus, the kinetic temperature can be obtained from the comparison of column densities derived for different transitions with different lower state energies. For example, the ratio of the ground state population to that of a fine structure state gives the excitation temperature, T_{ex}. This is well illustrated by the comparison of the two CII UV resonance lines (1334, 1335 Å). In a sequence, lines arising from different ground state multiplets of the same ion provide an ensemble of estimates of the electron temperature (or radiative excitation by the fine structure transitions). Since the latter is quite unlikely, given the low transition probabilities for those lines, the electron excitation dominates.

For the same ionic species, the set of available lines all have different gf values. If they are all resonance lines, each should have its own rate of saturation so taken together they provide a curve of growth. This is a simple means for visualizing the dependence of the equivalent width on the total τ. By including lines from excited states from the same ion, the line strengths are modulated by the term $\Delta E_i/kT_{ex}$. Multiplets have the same T_{ex}. The resulting integrated line strength is, however, very sensitive to spectral resolution. Along the line of sight, different clouds have different temperatures. This has no effect on the ground state lines but for fine

structure lines, The differences can be sorted out only if the ground and excited state contributions in the same velocity interval can be treated separately.[9]

Thus, comparing two lines of sight through the same medium (should there be two separate point sources viewed close enough to each other on the sky) the equivalent width may differ if the intrinsic line widths differ. The integral measure is not sufficient to distinguish between different column densities and different dynamics unambiguously. Note that absorption line studies were the first means by which *clouds* were identified. These can be defined, based on this experience, as *coherent structures of enhanced density and/or optical depth discernible within a limited range in radial velocity*. In other words, much like clouds in an atmosphere, those in the ISM have a boundary across which some distinguishable feature(s) change(s) in a short distance. Since the meaning of "distinguishable" requires a change (at any velocity) of the optical depth, the physical change can be complex (density, ionization, opacity mechanism, velocity dispersion). For example, for the volume density this is the obvious, everyday meaning of a cloud—a region of higher local density that is isolated in space (hence in radial velocity). The line width, by construction, is due to the internal dynamics of the medium. If they follow a Gaussian distribution, whether kinetic or microscopic motions, the value is given by the sum of the individual contributions in quadrature. If, however, there are either multiple components along the line of sight or a more complicated velocity spectrum (such as turbulence, see Chap. 11), this line width will give a wrong estimate of the column density.

2.2.5 *Obtaining Column Densities from Emission Lines*

Emission lines from an optically thin transition do not follow a curve of growth (they don't saturate) but much of the analysis is similar to absorption lines. We can treat emission lines in the low frequency (Rayleigh-Jeans) limit by assuming that the excitation and kinetic temperatures are the same and ignoring collisional de-excitation. The emissivity is then $J_\lambda = \tau_\lambda B_\lambda(T_{ex})$ in approximate LTE. The conventional quotation of emissivity uses the brightness temperature integrated over the line width in velocity units so, over the FWHM ΔV, the column density of the *upper* level, N_j is

$$N_j = (T_{ex} - T_{bg})^{-1}\left[exp\left(\frac{h\nu}{kT_{ex}}\right) - 1\right]^{-1} \frac{4\pi^{3/2}}{(ln\ 2)^{1/2}} \frac{1}{\lambda^3}\frac{1}{A_{ji}} T_B d\nu. \tag{2.31}$$

[9] As an example, Jenkins (1996), Cardelli et al. (1989), Fitzpatrick and Massa (1990, 2007), and Savage and Sembach (1996) use the τ in individually chosen velocity intervals based on the ground state line to determine individual line of sight cloud properties.

Replacing $\Delta T_B \Delta V$ with the integral $0.935 \int T_B d\upsilon$ assuming again a composite Gaussian profile, we obtain the scaling law for the column density in terms of the velocity integrated brightness temperature

$$N_j = 24.1 (T_{ex} - T_{bg})^{-1} \left[exp\left(\frac{h\nu}{kT_{ex}} \right) - 1 \right]^{-1} \frac{1}{\lambda^3} \frac{1}{A_{ji}} \int \Delta T_B d\upsilon \quad . \tag{2.32}$$

The only novelty here is a change in vocabulary. Usually at shorter wavelengths, from the IR through UV, fluxes are expressed in physical units rather than temperatures but otherwise optical ground state emission is treated in much the same way, at least for fine structure lines.[10] Except for the terminology, expressing the intensities as temperatures, the principals are identical with a few exceptions. The exponential for stimulated emission can be neglected since, except at cm wavelengths, $h\nu \gg kT_{ex}$ for typical interstellar conditions. In general, since the spontaneous transition rates are so high relative to the downward collision rates and the background flux also high, the lines are seen in absorption and the resulting optical depth comes from the *lower* state column densities. Whether the line is formed by collisions or scattering, the emission is irrelevant for the lower states except when formed by a recombination cascade. However, at radio wavelengths, the rotational levels have energy separations of order kT_{ex} so collisional excitation is possible, resulting in emission lines. Note that the difference in line formation is essential. The background sources at millimeter and centimeter wavelengths, other than the Galactic nonthermal emission (and the CMB in the case of H_2CO) are not sufficiently intense that their source function overwhelms the emission.

2.2.6 An Example: HI—The 21 Centimeter Line

The HI "spin-flip" transition at 21 cm or 1420.40575177 MHz was the first spectral line detected in the radio part of the spectrum in the 1950s (Ewen and Purcell 1951; Muller and Oort 1951). With the exception of maser emission lines, it is the strongest radio spectral line, often visible in an oscilloscope monitoring the observations. An excellent review of the observations of HI in the Galaxy that have been made with this transition is by Dickey and Lockman (1990). We will limit the discussion to general considerations that are directly relevant to the diffuse ISM.

In the ground state of neutral hydrogen ($1s^2 S_{1/2}$) the proton and the electron each have an intrinsic magnetic dipole moment so the state splits between the

[10] Those transitions that are radiatively pumped or result from recombination cascades require a more complicated approach and we refer the reader to, e.g. Kaplan and Pikel'ner (1970), Osterbrock and Ferland (2006), or Draine (2011) for further discussions.

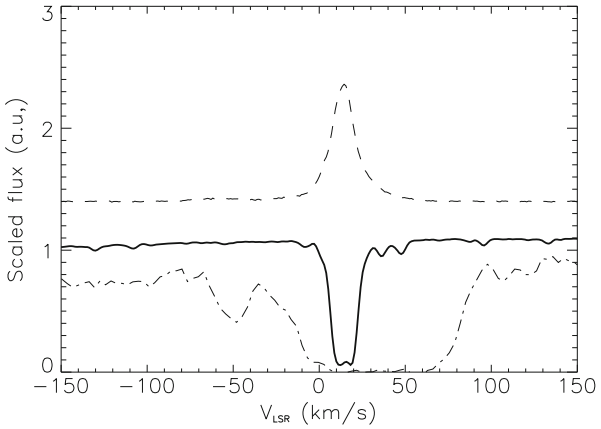

Fig. 2.4 An example of the neutral gas (NaI 5889 Å (solid black line) and OI 1302 Å (dot-dash-line)) compared with the 21 cm line emission profile (from the LAB survey—denoted by *dashed line*) along the line of sight toward the bright Galactic nova V339 Del. The clouds distinguished by the resonance metal absorption lines delineate a limited velocity range within the 21 cm emission, which is dispersed along the sight line beyond the star. The comparison of absorption and emission components in velocity constrain the E(B-V) through calibrations of the NaI D line absorption vs. reddening

parallel and antiparallel configuration with the latter having lower energy. These hyperfine sublevels are separated by $0.047\,\mathrm{cm}^{-1}$, corresponding to 0.7 K, and have statistical weights of 3 and 1 for the upper and lower levels, respectively. Any radiative transition between the levels changes the spin, so it is forbidden and the transition probability, A_{10} is very small: $2.85 \times 10^{-15}\ \mathrm{s}^{-1}$, equivalent to a lifetime of about 10 million years. The line is strong only because of the overwhelming abundance of atomic hydrogen in the ISM (see Fig. 2.4). Finally, the $n = 2$ or higher levels (the Balmer series) all lie more than $82000\ \mathrm{cm}^{-1}$ above the ground electronic state so their population in the neutral diffuse ISM is negligible (they are seen in emission only from recombination in HII regions or when the Lyman series is so optically thick that the levels are radiatively populated, which virtually never happens). Observations of the 21 cm line thus lead to very robust estimates of the atomic hydrogen column density. The excitation of the 21 cm transition is mainly by electron collisions. Excitation by the CMB can be ignored at typical interstellar densities and kinetic temperatures, Thus, in an example we cited earlier for collisional excitations, the excitation temperature for the 21 cm transition, also known as the *spin temperature*, T_s, is approximated by the gas kinetic temperature of the gas.

2.2.6.1 HI Emission

The line optical depth is $\tau \approx -ln(1 - \frac{\Delta T_B}{T_s})$ so when $\tau \ll 1$, the column density for the upper level is

$$N_u = 1.82 \times 10^{18} \int \Delta T_B dv \quad cm^{-2}. \tag{2.33}$$

If, instead, the line is optically thick, the column density is

$$N_u = 1.82 \times 10^{18} \int \Delta T_B \frac{\tau}{(1 - e^{-\tau})} dv \quad cm^{-2}. \tag{2.34}$$

As we discussed in Chap. 1, the diffuse ISM is partly atomic and partly molecular. Consequently, a complete view of the medium perforce requires molecular spectroscopic observations along with those at 21 cm.

The atomic gas not only envelops the molecular clouds (the outer parts of the PDRs), it is also mixed within the molecular gas. This neutral atomic gas is detected via "HI narrow self-absorption" lines or HINSA (Li and Goldsmith 2003), although the H^o density in the HINSA regions is about 1.5×10^{-3} that of the molecular gas (which is most likely around $10^3\,cm^{-3}$). The atomic component in dark clouds is produced by cosmic rays destroying H_2.

In emission, the problem of studying the HI distribution is primarily one of angular resolution. For example, at 21 cm, the Arecibo radio telescope has a relatively coarse resolution of $\sim 4'$. All-sky surveys of HI, such as the Leiden/Argentine/Bonn (LAB) survey (Kalberla et al. 2005) have even worse angular resolution, about 0.6 degrees. This is larger than the size of many diffuse molecular clouds and renders atomic-molecular comparisons approximate at best. Despite these difficulties, studies of the HI distribution around the lower-density molecular clouds can yield interesting results (e.g., Gir et al. 1994; Moriarty-Schieven and Wannier 1997). For example, in some instances the atomic gas envelops the molecular gas as in the case of MBM 40 (Shore et al. 2003), while in other cases the HI peaks to one side of the principal molecular emission (e.g., see Fig. 1.6, bottom right panel; Fig. 9.2, bottom right panel; and de Vries et al. 1987). However, improvements in resolution hold the key to understanding in detail the relationship between the gas components of the diffuse ISM.

Savage et al. (1977) established that in regions where E(B-V) < 0.1 mag the hydrogen nucleons were almost entirely atomic and the relationship between $N(H_{total})$ and E(B-V) could be expressed as

$$N(H) = 5.8 \times 10^{21} E(B - V) \qquad cm^{-2}. \tag{2.35}$$

This relationship was derived from Lyα observations toward early-type stars and is used extensively by astronomers (see Sect. 6.3).

All-sky maps of the neutral hydrogen sky provide the column density of HI in any direction albeit usually at somewhat poor resolution. The LAB HI survey (Leiden/Argentine/Bonn Galactic HI survey (Kalberla et al. 2005).[11] Covers the entire sky at a resolution of $\sim 0.6°$. The survey merges the Leiden/Dwingeloo survey by Hartmann and Burton (1997) with that of the Instituto Argentino de Radioastronomia. Covering a velocity range of $\pm$ 400 km s^{-1} at a velocity resolution of 1.03 km s^{-1}, the survey has an excellent rms noise in brightness temperature of 0.07–0.09 K and is corrected for stray radiation (see Sect. 4.2.5). With the most extensive coverage both spatially and kinematically and excellent sensitivity, this survey's only flaw is the relatively coarse spatial resolution. Another notable HI survey is HIPASS (the HI Parkes All-Sky Survey) with most of the data taken with the CSIRO 64-m Parkes Telescope. The survey covers the entire southern sky as well as declinations in the Northern Celestial Hemispher up to $+25°$. With a spatial resolution of 15.5′, a velocity coverage of $-1280 < cz < 12700$ km s^{-1}, and a velocity resolution of 18 km s^{-1}, the survey is best suited for extragalactic HI studies because the bandpass correction renders the Galactic signal virtually unusable for dynamics (each spectrum has the median signal from a declination strip 4° in length centered on the declination of the position subtracted from it). Finally, the Arecibo GALFA (Galactic Arecibo L-Band Feed Array) HI survey (Peek et al. 2011) provides the best resolution in a wide-field HI survey (3.5′), but the coverage is limited to what can be observed from Arecibo ($-2° \leq \delta \leq 38°$). Nevertheless, 13000 square degrees of sky will be covered once the survey is complete, at an excellent velocity resolution (0.18 km s^{-1}) and with excellent sensitivity (80 mK rms in integrated 1 km s^{-1} channels).

2.2.6.2 HI Absorption

Because HI can be found in every direction, there will be plenty of continuum sources that will show HI absorption. If we go back to the radiative transfer equation in the Raleigh-Jeans limit (equation 2.18) we can rewrite it as

$$T_B(\nu) = T_s[1 - e^{-\tau(\nu)}] + T_c e^{-\tau(\nu)} \tag{2.36}$$

where T_s is the 21 cm excitation temperature and the continuum temperature, T_c, replaces the background temperature, T_{bg}. Here $T_B(\nu)$ is just the on-source measurement and not $\Delta T_B(\nu)$. If we assume that the optical depth of the HI is small, then the above equation becomes:

$$T_B(\nu) = T_s\tau(\nu) + T_c[1 - \tau(\nu)] \tag{2.37}$$

[11] http://lambda.gsfc.nasa.gov/product/foreground/LAB_HI_Survey_info.cfm.

If we denote the depth of the absorption line as $T_L(\nu) = T_c - T_B(\nu)$, we can rewrite equation 2.37 as

$$\tau(\nu) = \frac{T_L(\nu)}{T_c - T_s}. \tag{2.38}$$

Compare this formulation to that of equation 4.3 that allows for the determination of the optical depth of atomic hydrogen from on-off observations.

2.2.6.3 HI Absorption Continuum Measurements

There is yet another way to obtain information about the column density of neutral hydrogen, and also heavy elements such as the CNO group, using X-ray observations. Although still in development (e.g., Gatuzz et al. 2016) using *XMM* and *Chandra* X-ray band spectroscopy and *Swift* X-ray and UV photometry work rather well in discriminating continuum absorption intrinsic to the source and that from the gas along the line of sight. The idea is quite straightforward. Absorption above the Lyman limit decreases rather slowly with energy so even in the soft X-ray spectral range the neutral gas has an optical depth $\tau(E) \approx \tau_{LyC}(E/13.6eV)^{-3}$. Studies of explosive events, such as classical novae, show that the minimum N_H obtained from the X-rays equals that inferred from the Lyα and other UV and optical resonance transitions. From spectrophotometry, the absorption edges of heavy elements can be studied independent of the line excitation conditions. Finally, using X-ray sources, mainly supernova remnants and low mass X-ray binaries observed in the continuum, Güver and Özel (2009) derived an alternate relation between atomic hydrogen column density and extinction, $N_H = (2.21 \pm 0.09) \times 10^{21} A_V$ (see Chap. 6). The method is very close to that used for the relative abundances based on the Lyman series.

2.2.7 *Line Pumping by the Cosmic Background Radiation: The Optical CN Transitions*

There is one important case, however, where the occupation of the levels responsible for diffuse phase optical transitions are radiatively determined by the far infrared background. This was discovered when McKellar (1940) and Adams (1941) identified the two ground state rotational lines of CN in coude spectra. McKellar's study was made possible by Herzberg's contemporary laboratory studies, and his paper included a discussion where it was noted that the rotational excitation of the lowest CN states in absorption correspond to $T_{ex} = 2.3^{+1.1}_{-0.7}$ K, depending on the uncertainties in the R(1)/R(0) line ratios. In a lengthy section in his 1941 paper, McKellar included questions about the applicability of LTE to such an environment, but argued that the ubiquity of this anomaly indicates the presence

of a universal exciting continuum and refers to Eddington's estimate of the mean radiation energy density resulting from a diffuse interstellar radiation field McKellar (1941).[12] When Alpher, Herman and Gamow were exploring the consequences of Big Bang cosmology for the production of the light elements, their predictions of possible residual emission from a primordial high temperature state were in the same range but they made no reference to the CN result.[13] The result re-appeared only after the detection of the cosmic microwave background by Penzias and Wilson in 1965. In back-to-back papers, Field and Hitchcock (1966a) and Thaddeus and Clauser (1966) explicitly cited the CN temperature as an indicator of the intensity of the CMB at 2.63 mm. Field and Hitchcock (1966b) went farther, showing that the CN supports the idea that the background radiation is not a manifestation of the DIRF (hence, finally, removing the conundrum raised by McKellar).

2.2.8 *Collisional Excitation in a Nearly Collisionless Medium*

Observed interstellar atomic transitions are either from the ground or fine structure states. The densities in the diffuse gas are so low that collisions are too infrequent to establish significant populations in the more highly excited states. The lines formed by absorption are therefore directly proportional to the column density of the ion. For molecular absorbers, however, this is more complicated. Rotational transitions of diatomic molecules have typical separations of a few hundredths of an eV, near the thermal velocity of the ambient particles (especially electrons). They are, therefore, potentially excited and the lower state populations reflect the thermal distribution of the gas, forming a rotational excitation ladder. In the absence of a strong radiation source, and in an optically thin medium, the populations of successively higher levels will relax to a Boltzmann distribution for which the excitation temperature approaches the kinetic temperature of the ambient perturbers so the logarithm ratio of column densities for the successive lines should be proportional to $\Delta E_{ij}/kT_{ex}$ where $\Delta E_{ij} \rightarrow \Delta E_{J,J+1} = (J+1)/I$ for dipole transitions from rotational levels J to $J+1$ and I is the moment of inertia. Vibrational states are more widely separated and may not be excited in the lower densities or by the cold gas. When the gas is optically thin, emission lines arise from the cascade to the ground state and the intensity ratios again follows the exponential distribution.

[12] In the last chapter of Eddington's 1926 tome *The Internal Constitution of the Stars*, he had speculated on the mean energy density of the space between the stars based on their diffuse radiation and computed an equivalent temperature for matter in thermal equilibrium that was similar to the excitation temperature required from the CN measurements.

[13] Ned Wright (http://www.astro.ucla.edu/~wright/CMB.html) called attention to the only pre-1965 reference to the possible cosmological implication of the CN detection. It is a review of one of Gamow's books by Hoyle (1950) that notes that the inferred relic radiation from the epoch of primordial nucleosynthesis was too hot compared to the CN excitation temperature. Nobody else noticed.

Collisions also establish a thermal distribution between fine structure levels if sufficiently frequent, as happens in the denser diffuse clouds, so the column density ratios are approximately the ratio of the statistical weights of the levels. This is not, however, always the case; for example, the ratio of the two fine structure states of hydrogen. For H_2, the ground state potential, $^1\Sigma_g$ comes in two forms, symmetric and antisymmetric in the nuclear spins, which are degenerate except for the rotational transitions. These are, alternately, positive for the odd J states and negative for even J. The ratio of these should be the ratio of the nuclear spin statistical weighs (the ortho- to para- ratio), which for $I = 1/2$ is either 1 or 0, hence the ratio of the statistical weights of 3:1 results when collisions produce a thermal statistical distribution. There are no radiative transitions between these. It is likely however, that the formation of H_2 leaves a mark on this ratio since it departs from the canonical value in dense media (see the discussion of astrochemistry in Chap. 3). Fine structure atomic transitions, of which the far infrared lines such as [CII] 158 μm is typical, are like the 21 cm line. They have very small transition probabilities and are not seen in absorption. But emission occurs when collisions excite the upper state and are not sufficiently frequent to de-excite the gas without emission of a photon. The same holds for the 21 cm line.

Line formation in the diffuse ISM is rather different from an atmosphere in another respect since there is no feedback from the radiative to mechanical properties of the gas. Emission following collisional excitations cools the gas but, when self-gravity can be safely ignored, the dynamics are unaffected by this (although the internal energy decreases, since pressure gradients are not responsible for structuring the equilibrium there is no dynamical consequence of this cooling). The electrons (and other perturbers) lose kinetic energy but this has no affect on the structure of the medium.

The diffuse gas is not strictly collisionless, as emission in neutral hydrogen at 21 cm demonstrates. The formation of this line is especially simple so we will use it as a prototype. The excited state has a very long lifetime, $A_{21} \approx 2.8 \times 10^{-15}$ s^{-1}. Since the B-value is proportional to this, the absorption coefficient follows immediately, $\kappa_{HI} \sim B_{21cm}$, the optical depth is linear in the column density of the ground state, and column densities of order 10^{21} cm^{-2} or higher are required for this to become optically thick. The transition is usually seen in emission, which might seem puzzling since it is not a scattering line like Lyα and with so low an absorption coefficient one would expect no radiative excitation. But there is an alternate, collisional channel for excitation. If the collision rate is $n_e C_{ij}$, where the rate coefficient depends only on temperature, then it suffices that the electron density be sufficiently low that detailed balance is not achieved to insure that a collisional excitation is followed by a radiative de-excitation. This condition gives the population ratio

$$n_j/n_i = n_e C_{ij}/A_{ji} \tag{2.39}$$

that, because of the extremely low thermal threshold, 0.1 K, guarantees collisional population of the upper state anywhere in the ISM. Thus, without some collisional excitation from electrons, the line would be observable only in absorption against Galactic and extragalactic nonthermal sources and then only very weakly given its minuscule oscillator strength.

The same reasoning can be applied to the fine structure of the resonance multiplets. Take, as an example, two of the dominant ions in the ISM, CII 1334, 1335 Å and MgII 2796, 2803Å. The former is a multiplet with the resonance line being $^2P^o_{1/2} - ^2D_{3/2}$ while the longer wavelength component is a $^2P^o_{3/2} - ^2D_{5/2}$ transition arising from a level 63 cm^{-1} above the ground state. The difference corresponds to the wavelength of the CII fine structure line, $^2P^o_{1/2} - ^2P^o_{3/2}$ at 157.7μm. If there is no absorption to the excited level, without collisional excitation there will be no emission in this infrared line. On the other hand, electron collisions can easily excite the upper state, increasing the optical depth of 1335 Å relative to the 1334 Å line. The fine structure line has a transition probability of $A_{ul} = 2.29 \times 10^{-6}$ s^{-1} so it is collisionally suppressed for densities above about 10^3 cm^{-3} (depending on the temperature, see below), but at lower densities it is radiatively de-excited and observable in the far infrared. This also illustrates the important role these fine structure lines play in the cooling of the clouds and the CNM. Their optical depth is negligible so any collision in the diffuse medium will be followed by emission of a freely escaping photon. The contrast is with MgII.

The two ultraviolet lines of MgII arise directly from the ground state and the separation from the first excited level is too large to be accessible to collisional excitations (it requires about 4 eV). Thus, the ratio of the optical depth of the two components of the line depends only on the column density of Mg^+. The same holds for the principal optical doublet of NaI 5889, 5893 Å. The two components are both from the ground state and their ratio is used as an extinction proxy. These, and CaI 4226.7 Å a singlet, and the doublet KI 7664.5, 7688.9 Å, are the only neutral atomic species of sufficient abundance to leave a signature on the spectrum. The other important optical ionic transition, CaII 3933, 3968 Å, is also a pair of ground state lines.

Electron excitation also affects the optical CN rotational transitions R(0) (J = 0 − 1)and R(1)(J = 1 − 2) . These are principally excited by the cosmic background radiation at 1.3 mm and 2.6 mm and should give an excitation temperature of $T_{CMB} = 2.725484$ K $\pm$ 570 μK Fixsen (2009). Gamow originally cited this line ratio as evidence for a FIR excitation by a cosmic radiative background. Ritchey et al. (2011) show, however, that the excitation exceeds what would be possible from radiation alone. For the diffuse cloud in the line of sight to HD 154368, they found an excess of about 63 mK. Since the exciting window is a minimum for Galactic thermal and synchrotron emission, even a difference of a few percent becomes significant. Harrison et al. (2013) show that electron collisions can account for the added populations within a relatively narrow density range in the diffuse medium, $n_e \approx 0.01$ to 0.06 cm^{-3}. This is on the low side for the mean density but quite in line with the expected range of fluctuations. The excitation cross section peaks at around

20 K . Similarly to the 21 cm line, weak emission has been detected in the hyperfine structure transition ($N = 1, F = 3/2, J = 5/2) - (0, 1/2, 3/2)$ at 113.49 GHz (Palazzi et al. 1990) with a brightness temperature of about 20 mK.

2.2.9 *Dynamical and Nonlocal Complications to Radiative Transfer*

2.2.9.1 Escape Probability and Photon Trapping

The equivalent width is the cumulant of all absorption along the line of sight to a source within the velocity range of the line profile. If the observed line is due to only one component, W_λ depends on a unique column density and the analysis proceeds as we have outlined. If, however, there are many individual absorbers, such as a string of clouds toward a background source each moving with a different center of mass velocity and unrelated to each other, the optical depth at each wavelength is the sum of all components capable of absorbing at the observed velocity. This is problematic for UV, optical, and IR spectroscopy where the resolutions are limited to about 0.5 km s^{-1}. For mm wavelengths this is not a problem since current autocorrelators easily achieve resolutions of less than 0.05 km s^{-1}. Unless we can separate the individual contributions, we do not know from a single profile what might be the differences from one absorbing system to another (see Jenkins 2009). It is now well established that above helium, the atomic phase is differentially depleted by adsorption on dust. If one only observes the line of sight total absorption, and the profile appears monolithic, only the total depletion can be measured. But depending on the local conditions, depletion is more effective in dense than rarefied clouds. So without being able to separate individual velocity coherent structures, even a comparison between lines of the same species may be misleading. To see this, think of two lines from the same ground state, one stronger than the other (they have different *gf* values, e.g. the doublets NaI D1 5895 Å, D2 5889 Å or CII 1334, 1335 Å). At large column densities the stronger component saturates first for a single constituent absorber (e.g., Wilson and Merrill 1937). But both line components may be unsaturated because of differential absorption in individual line of sight structures, some of which may be intrinsically more transparent and others less so. The component ratio is conventionally taken as a direct indicator of optical depth, hence it would normally be used to get N, the column density. The equivalent width is, however, an integral measure over the whole velocity range covered by the profile so the ratio of the components may yield the wrong optical depth. Recall that the line of sight contributors to τ add linearly, an ensemble of profiles produce, at some ν, a total

$$\tau_\nu = \Sigma_i \tau_{0,i} \Phi(\nu - \nu_{0,i}; \sigma_i) \tag{2.40}$$

where σ_i is the velocity dispersion of the i^{th} component whose optical depth at line center is $\tau_{0,i}$.

The problem arises when either the velocity dispersion or the column and volumetric densities are different in each component. Densities of a particular species can change because of differential elemental depletion, while possible differences in internal dynamics change the dispersion and skew. The line *shifts* may be systematic, because of Galactic rotation separating clouds along the line of sight that are possibly distant from each other, or there can be large scale random motions of similar magnitude as the differential rotation, or the changes may come from superposition of small individual absorbers which are in the same dynamical complex but otherwise unrelated to each other. Hence a word of caution: all these effects are conflated in unresolved profiles.

Escape probability methods have the intuitive appeal of following a photon on its journey through the obstacle course of a medium. Although it is less important for treating line formation in diffuse, optically thin environments, when the column densities become sufficiently high escape probability makes the concept of *photon trapping* easier to grasp. As we discussed in Sect. 2.2, the penetration probability for a photon along an arbitrary line of sight is an exponential in the optical depth. But we sometimes want to know what the likelihood is that it will *escape* from some internal point, for instance when treating the cooling of a cloud or calculating the volumetric emissivity of a structure. Such questions involve integrating over all possible paths and are particularly important for correctly accounting for radiative losses from denser environments. Remember, "optical depth unity" is just another way of specifying that the photosphere is for a bounded structure. We are interested in the radiation escaping from a medium so the relevant quantity is the flux originating at some depth τ. Imagine, for illustration, a finite thickness slab for which the total optical depth is τ_0. Photons can exit at any angle so they see along any direction a scaled optical depth τ/μ where μ is the directional cosine relative to the surface normal. In a (horizontally) infinite slab, those trajectories parallel to the surface see ahead of them an infinite line of sight τ so they can only escape if deviated. Otherwise, at any point in the medium they will surely be absorbed. The escape probability is obtained by integrating over all directions

$$p_{esc,\nu} = \frac{1}{\tau_{0,\nu}}(1 - e^{-\tau_{0,\nu}}) \tag{2.41}$$

where now we explicitly include the frequency. In the limit of small τ_0, $p_{esc} \rightarrow 1$ and varies as τ_0^{-1} for large τ_0. Slabs are rather poor models for clouds, although they are good approximations to PDRs. For a sphere, the maximum optical depth in any line of sight through the sphere is $\tau_\nu = \tau\mu$ with $\mu = \cos\theta$ being the direction cosine. Then, if the center of the sphere has an optical depth τ_0, we can write

$$F_\nu \sim \int_0^1 T_{ex}[\exp(-\tau_{\nu,0}\mu)]\mu d\mu. \tag{2.42}$$

In the limit of infinite optical depth this quantity vanishes, when $\tau \rightarrow 0$ it goes to unity. This provides the *escape probability* for a photon emitted from some optical depth reaching the surface of the cloud. A systematic velocity gradient makes an enormous difference. When the linewidth given by what we can consider to be microscopic processes (whether thermal or small scale homogeneous turbulence) is smaller than the gradient of the macroscale motions along any line of sight (for instance, for an expanding medium) the optical depth decreases and the escape rate goes up.

For a cloud with an internal source function $S_\nu = j_\nu/\kappa_\nu$ where volume emissivity is j_ν, replacing κ_ν by the optical depth gives $S_\nu = j_\nu/(\tau_\nu/R)$ for a radius R. The escape probability is the ratio of the emerging flux from some optical depth to the total emitted from the volume so from equation 2.41

$$p_{esc,\nu} = \frac{3}{8\tau_\nu^3}[2\tau_\nu^2 + (1 + 2\tau_\nu)\exp(-2\tau_\nu) - 1]. \tag{2.43}$$

The important feature here is that the optical depth is the maximum through the sphere that depends on the column density. The formalism is therefore an integrated measure and valid at each frequency. The line profile now enters since p_ν must be averaged over the profile. Since for a velocity gradient the optical depth at line center decreases, the escape is enhanced. Instead, turbulence, while it decreases the opacity at line center, enhances that at large displacement from ν_0 so the effect (for fully developed microscale motions) is the same as a broadened Gaussian. A different spectrum, for instance a power law in scale as we will discuss in Chap. 11, changes this.

2.2.9.2 Velocity Gradients and Line Transfer

The monochromatic optical depth depends on the total line of sight absorption at *a specific point in the line profile*. For a static medium, the absorption line profile is symmetric around line center. If, instead, the medium displays velocities that are coordinated on longer distances than a photon mean free path, the centroid also shifts and the opacity at any point in the profile now depends on how these shifts occur along the line of sight. Take the example of a line that is thermally broadened on the microscale but that is formed in a uniformly accelerating mass flow. Since we have no constraint that an interstellar cloud is hydrostatic, there can be a net divergence in some volume. Alternatively, the flow can have a complex (but not chaotic) pattern in three dimensions (shears, twists, and the like). A photon is emitted at some frequency $\Delta\nu$ relative to line center at point A, the rate depending on $\Phi(\Delta\nu)$ as we discussed earlier. It then, statistically, goes straight ahead until it hits something, say a molecule in the ground state, at another point B. The mean free path would normally be $[n\kappa_0\Phi(\Delta\nu)]^{-1}$ were the profiles the same. But in a larger scale flow, there is a Doppler shift, $\Delta\nu_D = \nu_0(\mathbf{v}/c)\cdot\hat{\mathbf{k}}$ that displaces the B profile relative to A by some $\Delta\nu + \Delta\nu_D$ that may increase or decrease the line of

sight opacity relative to the static case. Thus, the mean free path changes. The effect is easiest to see for a Gaussian, where the line width is σ. If $\Delta v_D \gg \sigma$, then the velocity shift *statistically* decreases the opacity and increases the mean free path. This is called the Sobolev or "on-the-spot" approximation. The effect of changing the mean velocity is the same as altering the column density but in a subtle way. If the flow changes its orientation relative to the observer, the optical depth can change abruptly.[14] If a molecular cloud is sufficiently dense it may have a "photosphere" in the far infrared but, in general—and especially for diffuse and translucent molecular clouds (see Chap. 9)—they are transparent in the continuum. Instead, the absorption is seen only against the line emitting region itself. Any part of the flow that is opaque along the line of sight leaves an imprint on some part of the profile at its specific velocity and self-absorption can occur because a change in the velocity or density produces an increase in the line of sight optical depth.

We will return to the issue of random flow fields when discussing turbulence in Chap. 11. But it is useful to make a remark here concerning the difference between a smooth and chaotic velocity field. In the disorder of turbulence, the macroscale is covered by a broad range of fluctuations in both density and velocity (and temperature, but for now we will assume isothermality). The optical depth in the line is simply redistributed over a broader bandpass and the line core becomes more transparent. Since in emission the photons are most likely to emerge from the core, turbulent reduction of the optical depth at line center increases the radiative losses. A diagnostic of the opacity is usually isotopic ratios. Since the chemistry cannot produce unlimited enrichments of rare species, for instance the ^{13}CO/^{12}CO ratio, the more abundant species is also the less transparent. Thus, if the optical depth increases, the ^{12}CO lines saturate first. Note that were there a continuum against which to absorb, the total velocity-corrected column density could be directly measured. But since the only source function is line emission, the broader the profile the less easily the opaque regions can be identified.

The comparison shown in Figs. 2.5, 2.6, 2.7 of two different lines of sight through the Galaxy illustrates how the optical depth depends on the excitation conditions. The lines are resonance transitions observed against two bright Galactic novae, V339 Del 2013 ($\ell, b \sim 62.2°, -9.4°$) and T Pyx 2011 ($\ell, b \sim 257.2°, +9.7°$). Both were unassociated with any star forming region, and were merely passive

[14]This is most familiar from stellar winds where, near the terminal velocity, the radial velocity gradient asymptotically vanishes. Despite the decreasing number density, the effective optical depth can produce saturated absorption up to nearly the maximum velocity of the flow. This is the familiar P Cygni profile characteristic of mass outflows. This effect is also strongly nonlocal since very distant zones of the flow can now communicate through absorption. In contrast to an interstellar flow, that in a wind is mainly radial with an optically thick surface at the lower boundary. Consequently, the absorption is always shifted to the blue and the emission, on the redward side of the line, is always optically thin. There is always a surface from which a broadband continuum emerges against which the absorption occurs. The relative intensity of absorption and emission (for complete coverage by a spherical outflow) is set by the ratio of the solid angle subtended by the outer regions of the wind to the photosphere.

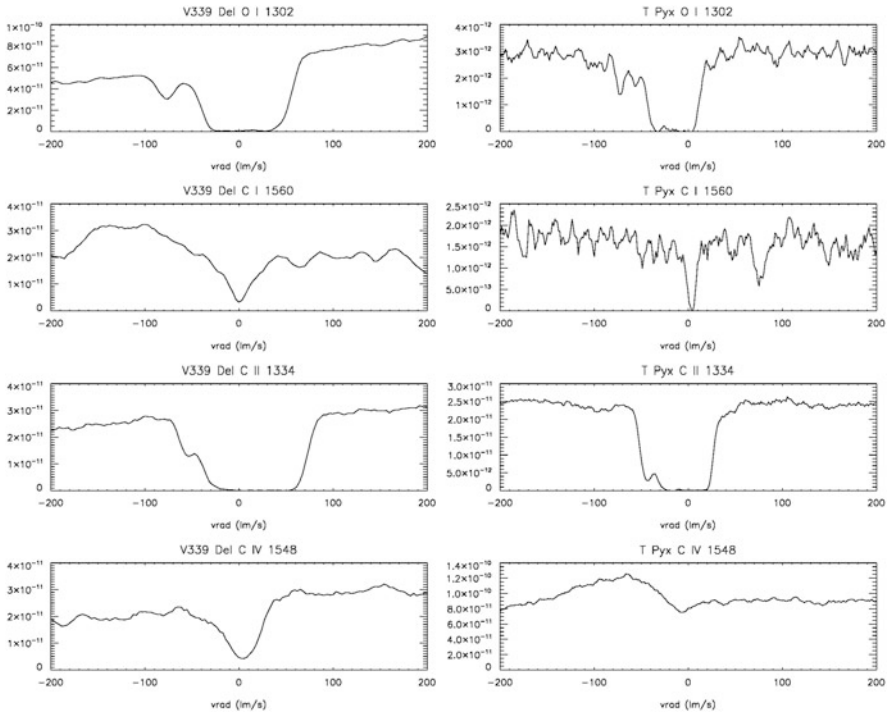

Fig. 2.5 Absorption lines along the line of sight to the nova V339 Del on the left and T Pyx on the right. The species and the wavelength (in Å) of the depicted transition are labeled above each spectrum. The spectra were taken with the Space Telescope Imaging Spectrograph (STIS) on the Hubble Space Telescope

background sources whose spectra were time variable. Hence, it was easy to distinguish the interstellar from stellar lines.

A number of important molecular species also absorb at optical and ultraviolet wavelengths, and were first identified long before millimeter wave astronomy became available for studying molecules in the diffuse phase. The observed lines, representing the species CN, CH, CH^+, HCO^+, and CO, are vibrational-electronic transitions. An example of such excitation are the H_2 bands formed by absorption from the ground state $X^1\Sigma_g^+$ to the two excited states $B^1\Sigma_u^+$ (Lyman band) and $C^1\Pi_u$ (Werner band) electronic states (Abgrall et al. 1993) which is, in fact, the *only* way to directly observe this essential species in the cold neutral medium in absorption (noting that the molecule is symmetric and has no dipole transitions, a point to which we will repeatedly return). The absorption is observable only in the vacuum ultraviolet (VUV), the Lyman band lies below 1108 Å and the Werner band is below 1008 Å, so until the 1990s, using spectra obtained with *FUSE*, only a few select lines of sight were available at high enough resolution to study the gas distribution (using *Copernicus* spectra, see Savage and Sembach

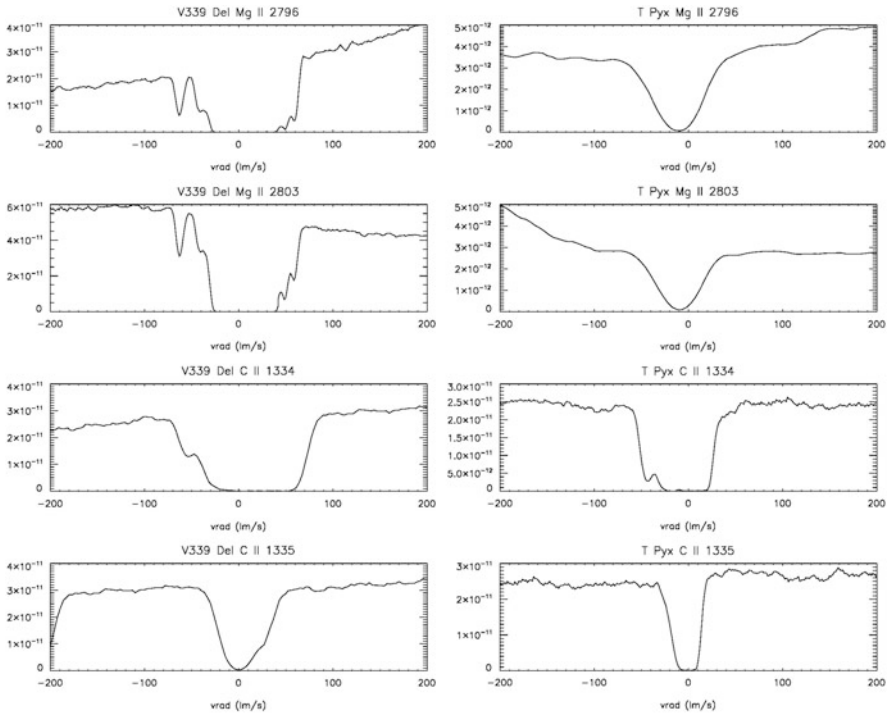

Fig. 2.6 Same as Fig. 2.5; additional absorption lines along the line of sight to the nova V339 Del on the left and T Pyx on the right

1996). The lines occur in emission by two mechanisms. If the colliding electrons have sufficient energy to excite the rotational lines of the $v = 0 \rightarrow v = 0$ system with $\Delta J = 0, \pm 2$ but this is not normally the case in the diffuse ISM. In shocked gas, where the velocities are above a few tens km s^{-1}, rotational lines from the ground state are excited. For $\Delta v = 1$, requiring 0.5 eV, rotational lines can also be excited but the shocks must be much stronger (with velocities > 25 km s^{-1}). In all cases, the essential requirement is that the collisions not be sufficiently energetic to dissociate the H_2, which requires about 4.5 eV. Although this is far higher than the $\Delta v = 1$ excitation, the destruction of the molecule is not balanced by rapid re-association. Alternatively, absorption in the neighborhood of strong UV sources pumps the excited states that decay radiatively. But, in general, the lines are observed in absorption.

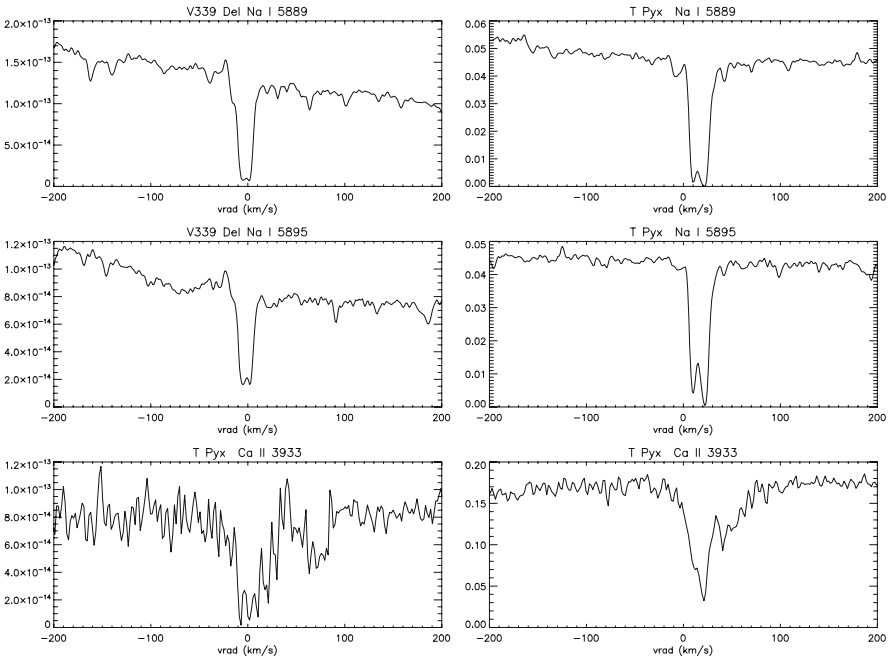

Fig. 2.7 Same as in Figs. 2.5 and 2.6; additional optical absorption lines along the line of sight to the nova V339 Del on the left and T Pyx on the right

2.2.10 Elemental Abundances and Depletion in the Diffuse Medium

Absolute elemental abundances are not the same as ion column densities. To achieve a comparison with stellar values, the ionization state must be known. In general, only one or two ions are observed for most species for the diffuse medium in currently available wavelength ranges. For instance, nitrogen has only N^0 and N^{+4}, oxygen shows only the neutral lines like Na, and the same applies to Mg and Ca. Carbon and silicon are better represented, and resonance lines are observable for the neutral through three times ionized states. This wide range is very important since their neutral state ionization potentials are lower than that of neutral hydrogen. As we will discuss, these are the major constituents of the solid interstellar phase, dust, so it is rather important to have some idea of how the abundances compare with those in stars. Stellar abundances are conventionally normalized to hydrogen—based mainly on the optical Balmer lines, but for the ISM, obtaining the hydrogen abundance is more difficult. For a start, the population of the parent state for the Balmer series is negligible in the ISM, unlike the far denser environment of a stellar atmosphere. The neutral hydrogen column density is available from the 21 cm line, but the emission line includes gas beyond the source. The resonance absorption

Table 2.1 Depletion factors in the diffuse medium for key elements (Jenkins 2009)

Element	$\log(X/H)_\odot$	f_{min}	f_{max}
C	8.46	−0.1	−0.21
N	7.40	−0.11	−0.11
O	8.76	−0.01	−0.24
Mg	7.62	−0.27	−1.36
Si	7.61	−0.22	−1.36
Fe	7.54	−0.95	−2.24
Zn	4.70	0.06	−0.55

lines of neutral hydrogen, Lyα 1215 Å and the rest of the Lyman series, sample the same gas along the line of sight as all other absorption lines toward a light source arising from the diffuse gas. But this measurement is not always possible or straightforward. The Lyman series lies in the VUV and *cannot* be observed from the ground. Additionally, hot luminous stars also show this line in the photospheric spectrum so sufficient resolution is required to permit separation of the stellar and interstellar components.

There are now several hundred lines of sight available from high resolution spectra. These show that the abundance pattern in the diffuse ISM is substantially different than the solar elemental distribution, a phenomenon called *depletion*. The dependence of the deficit on local conditions has been detailed by Jenkins (2009).

In Table 2.1, the depletion factors, measured as $\log(X/H) - \log(X/H)_\odot$ are indicated for different environments, defined by Jenkins (2009) as minimally and maximally depleted. The solar abundances are from a compilation by Lodders (2003) representing a best estimate of pre-solar system diffuse interstellar metallicities. We include Zn because it is well studied using strong resonance lines in the UV at 2054 Å and 2063 Å, analogous to the CII and MgII lines.

The ionization state of the gas is estimated by comparing the individual neutral and ion line profiles in velocity. Since the resolution is the ultimate limit to such studies, the ratio of column densities—hence, the ionization fraction for the heavy metal of interest—can be obtained within each component. The advantage is that the transitions are from the same element. While it is often impossible to determine the full ionization sequence, most of the doubly ionized species have resonance transitions in the FUV, the ionization state is mainly due to the neutrals and singly ionized species. A further feature of the absorption is that it can be used to check emission line studies for some diffuse regions. In HII regions, for instance, the column densities are sufficiently high that absorption from the diffuse gas toward the central stars is detectable in some systems. And it should be added that in addition to HII regions, supernova remnants (e.g. SN 1006) have been studied by this method in the ultraviolet.

To obtain the hydrogen column requires FUV observations of the Lyman and Werner bands for H_2 and those Lyman series lines for atomic hydrogen lying below 1100 Å that are available from archival FUSE or *Copernicus* spectra, and HI Lyα profiles from *HST*. The available Galactic directions are sufficiently broadly dis-

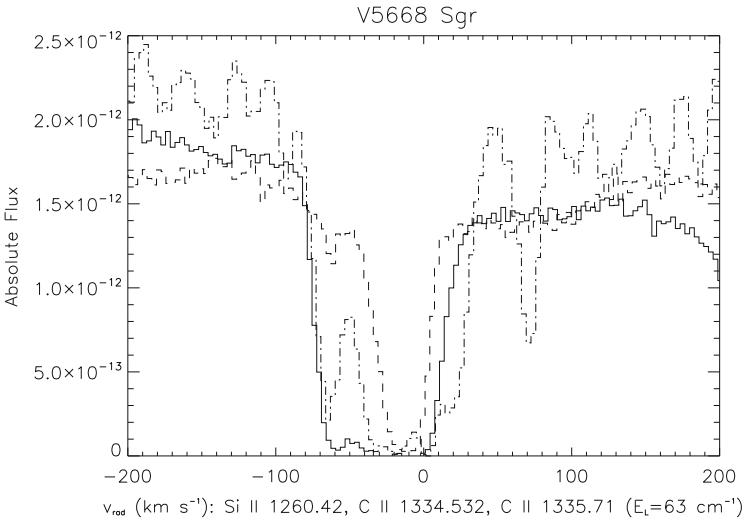

Fig. 2.8 Absorption lines along the line of sight to the nova V5668 Sgr 2015. The *solid line* is the CII 1334.532 Å line, the *dashed line* is the CII excited state, and the *dot-dash line* is the SiII. These spectra show the effects of effective excitation and were taken with the Space Telescope Imaging Spectrograph (STIS) on the Hubble Space Telescope

tributed that a representative abundances can be obtained. For the neutral hydrogen component, modeling the spectral energy distributions of X-ray sources provides estimates of N_H. Additional information has recently been derived from interstellar ionizing continuum absorption from C, N, and O but this is just beginning and is severely limited by the requirement that the hydrogen column densities cannot be too large. The advantage of this spectroscopy derives from the ability to separate individual components in radial velocity so the material conditions and column densities (and abundances) can be obtained even for individual clouds. Examples are shown in Figs. 2.8, 2.9, 2.10 for the line of sight to the classical nova V5668 Sgr 2015 ($\ell, b \sim 5.4°, -9.9°$). For instance, while SII is very strong in several transitions, there is no neutral sulfur along the line of sight, nor FeI. Neutral nitrogen and oxygen are quite strong but individual transitions are sensitive to different excitation conditions. The difficulty this poses for any abundance analysis is then evident: without the full set of available ionization states, only ionic column densities are available. Consider the case where the line of sight intersects several clouds. These may have nothing at all to do with each other yet contribute to the absorption in each velocity interval. Individual transitions of different optical depth help disentangling the components but this is critically dependent on the resolution and, therefore, can be confused with macroscopic broadening or turbulence.

Snow et al. (2002)—specifically for Fe along translucent lines of sight with FUSE—derive the mean number density by taking total H column densities and

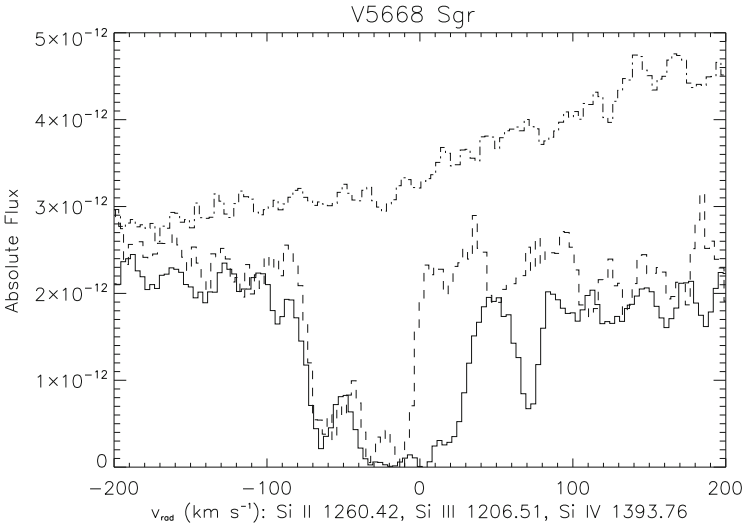

Fig. 2.9 Absorption lines along the line of sight to the nova V5668 Sgr 2015. The *solid line* is the SiII line, the *dashed line* is the SiIII line, and the *dot-dash line* is the nondetection of SiIV. These spectra show the effects of ionization differences in silicon and were taken with the Space Telescope Imaging Spectrograph (STIS) on the Hubble Space Telescope

dividing by distance, something that is possible for stars with known characteristics since these are absorption measurements.

2.2.11 H_2 and Fine Structure Transitions

One of the subtle conspiracies of nature is that the dominant species responsible for most of the mass of molecular clouds (helium atoms are not negligible in the mass budget of a molecular cloud) is intrinsically unobservable. Neutral molecular hydrogen has no permanent dipole moment so infrared emission from the lowest rotational and vibrational bands is strongly prohibited. There are, however, observable electronic transitions in the ultraviolet, in absorption, that can be viewed through translucent (but not dense) clouds: the Lyman and Werner bands.[15] This requires a background ultraviolet source (at this wavelength a relatively rare beast) that either has a long enough line of sight through the ISM or a high enough local density. In the former case, this requires distant massive stars or QSOs, although it is possible to observe. For nearby stars, hot subdwarfs, it requires high volume densities. This comes in the form of vibrational bands, all arising from the ground

[15]The Lyman bands are from the $B^1\Sigma_u^+$ to $X^1\Sigma_g^+$ and the Werner bands are from the $C^1\Pi_u$ to the $X^1\Sigma_g^+$ states, lying below 1100 Å (above 11 eV).

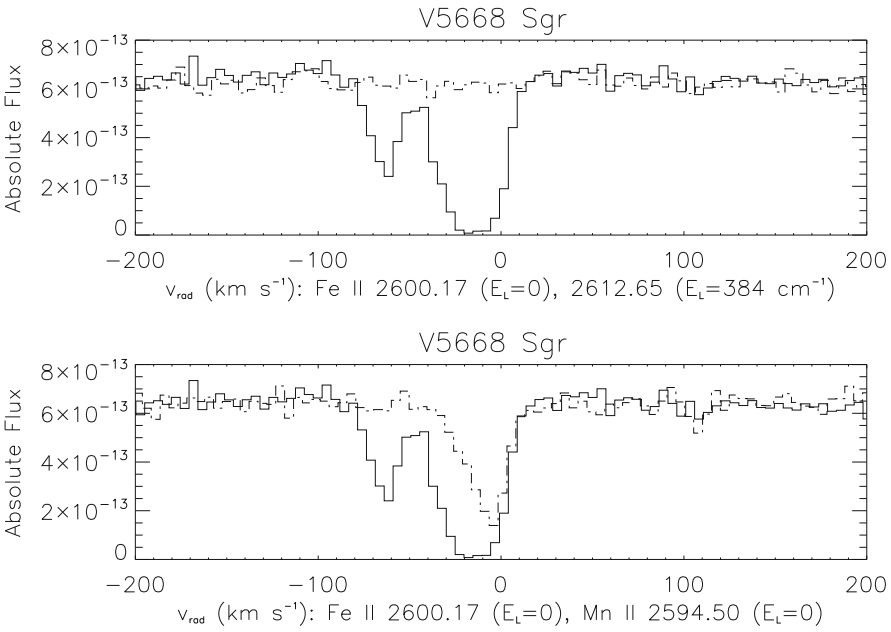

Fig. 2.10 Absorption lines along the line of sight to the nova V5668 Sgr 2015. In the top panel, the *solid line* is the FeII line at 2600.17 Å and the *dashed line* is the excited state. In the bottom panel, the *solid line* is again the FeII line at 2600.17 Å but the *dashed line* is the MnII 2594.50 Å line. The top spectrum illustrates excitation effects and the bottom differing abundances (both spectra arise from the same lower level). The spectra were taken with the Space Telescope Imaging Spectrograph (STIS) on the Hubble Space Telescope

state since the energy separation is about 0.1 eV ($T_{kin} \approx 10^3$ K for the vibrational states). The de-excitation, however, rather than leading to an emission band (again from the ground state) dissociates the molecule because of an intermediate energy, unbound $^3\Sigma_g^+$ state. This two step mechanism, first realized in the '60s (Stecher and Williams 1966) is the cornerstone for the formation of PDRs (see discussion in Sect. 1.7.1). But for our purposes, the most important point is that H_2 is nearly invisible—and certainly *is* so in the infrared and millimeter for the cold ISM. Thus, for molecular clouds, the presence of H_2 is an inference, not a direct observational detection, and its study depends critically on a chain of calibrations (see Chap. 8).

To further complicate matters, the interactions with CO are with a strongly dipolar molecule, that exists only in the neutral state. The interactions are, therefore, only weak and of a dipole-neutral type. The collision cross section is that of a pseudo-molecular state in which the perturber is weakly bound (the same as an autoionizing or pre-dissociating state).

This provides the excitation rate since there are few strong continuum sources at 1–3 mm in the Galaxy. Against extragalactic sources, there is a possibility of absorption but the flux densities are too low to balance the collision rates so that

is seen as an absorption along a line of sight toward a point source (however observations of this type have led to some interesting conclusions—see Sect. 7.4.3). As for the 21 cm line, we have the same excitation condition: every collision with a rate $n_{H_2} C_{01} n_0$ is followed by a radiative de-excitation with rate $n_1 A_{10} h\nu$. hence, the ratio n_1/n_0 depends on the kinetic temperatures (in effect, on $T_{ex}/T_{kin} \approx 1$ for the transition).

2.2.12 *Diffuse Interstellar Features in Emission and Absorption: Radiative Excitations and Fluorescence*

Even in the diffuse ISM, radiative processes alone can determine the spectrum if the collisions are sufficiently rare. This depends, however, on the properties of the radiation source. Take the example of the infrared diffuse emission features. These are due to C-H and C-C bond stretching of complex species. Their precise identification remains elusive, the same for the optical diffuse interstellar bands (DIBs, broad absorption features whose width cannot be either thermal or dynamical in origin—see 3.5.3). Complex molecules, those almost massive enough to show solid state band structures, are very efficient absorbers in the UV. In the diffuse interstellar medium, the global higher-energy-than-infrared radiation field resembles a star with an effective temperature of about 10^4 K. This emission extends beyond 3 eV, and PAHs are especially stable up to about 10 eV. Absorption against this diffuse UV continuum can excite electronic transitions, without ionization, that de-excite through vibrational bands in the near IR. The emission will, therefore, drive the radiation temperatures far above those in thermal equilibrium, as expected for larger dust grains. The process conserves photon energy but not number and the band lifetimes are so short relative to the collision frequency that the levels are far from thermal equilibrium. The emission was first detected in the IRAS cirrus and in reflection nebulae near hot stars.

Another familiar example of photon coupling is from IR pumping of transitions that can produce population inversions, hence *maser* emission. The optical depth is $\tau(\Delta\nu) \sim n_i B_{ij} - n_j B_{ji}$ so if there is a strong pumping of a third level whose decay overpopulates the upper state of a resonance emission line, τ can be negative. The medium then becomes an amplifier. The emission comes out within the natural line width and only couples within a very narrow range in velocity around line center. Thus, the pumping radiation is channeled from a broadband absorption into a very narrow emission with a consequent increase in brightness temperature. In the laboratory, this is usually referred to as a negative temperature but, since we have been strict in defining temperature as kinetic, connected with the thermal motion of the gas, there is no reason for invoking any arcane description: population inversion and emission line amplification are the signature of NLTE. The emission is extremely fine-tuned, any turbulence induced fluctuation can spontaneously lead

to desaturation of the maser along any line of sight. The same is true for large velocity gradients. So the region over which motion is coherent is the scale of the amplification length.

In 1920, Heger found a pair of weak, broad absorption lines in the spectrum of the B star ζ Per (and other B stars) at 5780 and 5797 Å that she suspected might be interstellar in origin (see Merrill 1938). The reasoning was the same as for the CaII and NaI lines: They appeared to have a different radial velocity than the photospheric absorption lines. Subsequent work by Merrill, Beals, and Greenstein among others added to the list and Beals added a number of such *diffuse interstellar bands* (DIBs) to the list, notably at 4430, 5778, 5780, 5796, 6177, 6196, 6284, and 6614 Å. Herbig (1975) attempted an analysis of possible carriers of the features based on their Galactic occurrence and wavelength distribution, going so far as to produce a tentative energy level diagram. But despite the best efforts over the past century, the identification of the responsible agent(s) remains an open problem (the most recent collection of studies, IAU Symp. 297 ends inconclusively).[16] The 5780, 5796 Å bands have also been observed in extragalactic environments, notably the LMC, M 31, and M 33 (e.g., Bailey et al. 2015). All surveys, whether of lines of sight within the Galactic or elsewhere, find a positive correlation between extinction (measured by E(B-V)) and the strength of the features but no single law for all of the bands. To further complicate matters, the individual bands do not all correlate with each other in strength. There are now over 400 cataloged features, some almost as narrow as atomic or molecular transitions, others having FWHM of many Ångstroms (see Tielens 2014) and varying in absorption depth from a few to almost thirty percent. An interesting feature is that they display a power law distribution for line strengths in single sources. The positive correlation with broad interstellar properties argues for a common atomic composition, mainly hydrogenated forms of C, N, and O bearing molecules but that is about all that is known. Only one species, the fullerene C_{60}^{+} has recently been firmly associated with two DIBs, [9577/9633 Å] by Campbell et al. (2015).

However, there is a related component of the ISM, the polycyclic aromatic hydrocarbons (PAHs hereafter) that are associated with emission bands in the near infrared (Tielens 2008). The detection of excess FIR emission from reflection nebulae stimulated the search for a large molecular origin of the bands. The bands arise from generic transitions, C-H and C-C bond stretching and various bending modes, and the originating molecules are difficult to distinguish from these observations alone. There is even a question about whether one is even possible.

Radiative excitation is rare in the diffuse medium since the diffuse interstellar radiation field has far too low an energy density to produce significant emission by direct absorption. There is, however, one exception that relates directly to the physical meaning of the source function. Solids have such an enormous number of available internal degrees of freedom that one expects the absorption process

[16] See, *Proceedings*, IAU Symposium 279, *The Diffuse Interstellar Bands*, eds. J. Cami and N.L.J. Cox, Cambridge U. Press (2013).

to lead to thermalized emission. So for large ensembles, such as dust grains, the emissivity should be a Planck function at the radiative equilibrium temperature. Hence, if the absorption coefficient is $\kappa_{\nu,D} = Q_{abs}(\nu)\pi a^2$, where a is the grain radius and Q is the efficiency factor (see Draine 2003), the emission spectrum is $j_\nu = \kappa_{\nu,D} B_\nu(T)$ and T is determined by the net absorbed flux independent of the spectral distribution. If, however, the grains are in the gray area between very large molecules and small solids, the absorption occurring in bands is followed by cascades through the allowed transitions back to the ground state in a time that is short compared to the arrival rate for the individual photons. Instead of a modified blackbody with the same brightness temperature at all wavelengths, the emitted spectrum will be a complex of bands whose individual intensities are generally far higher than expected from simple thermal emission. The complex is actually a line spectrum, a down-conversion of the absorbed photon distribution through the cascade. If the lines are not individually resolved but, instead, photometrically folded through a broad bandpass, the emissivity will exceed that measured at longer wavelengths and appears as an anomalously hot component. This is how the small grain component of interstellar dust was first detected (e.g. Sellgren 1983; Tielens 2008) from near infrared emission (first in reflection nebulae in the vicinity of hot but not ionizing stars, then in cirrus diffuse 12 and 25 μm band emission from *IRAS*). Although the process can be described as non-equilibrium thermal fluctuations in the grains, hence that the specific heat is temperature dependent, the emission is a manifestation of NLTE. The level populations are independent of the collision rates and produced by radiative equilibrium.

The emission mechanism is an extreme sort of fluorescence. Recall that the simplest version of this is a radiative excitation followed by a down-conversion cascade through lower lying states. The cascade is only interrupted by collisions if the transition probabilities are sufficiently low (the same criterion as forbidden line emission). The pump can operate in any spectral interval above that of the target levels. The emission from small grains, particularly those like PAHs and perhaps fullerenes, is a more complicated version of the simple conversion process. Having so many vibrational modes, the redistribution is a pseudo-continuum with the strongest emission concentrated at the main bands due to C-C and C-H bond stretch. The bands are broadened because of the large number of independent modes in the molecule.

The extinction curve in the UV is distinguished by a broad absorption feature at 2175 Å. This, however, varies across the Galactic plane with the two extremes being ζ Oph type for a strong bump and σ Sco for the weak feature.

2.3 Radio Continuum Measurements of the Diffuse Medium

The diffuse medium also modifies radio frequency signals because it is partially ionized and magnetic. The continuum processes are refractive and depend on electron scattering. They are, therefore, only frequency dependent because the

response of a medium (its characteristic frequency) is quite near the groundbased-accessible range. Centimeter and meter wavelength radio observations are also useful for probing the ionization and structure of the diffuse medium. The real part of the index of refraction for a radio signal (here we intend below 10 GHz or so) depends on the frequency and the plasma frequency, $\omega_p^2 = 4\pi e n_e/m_e$ as

$$n^2 = 1 - \left(\frac{\omega_p}{\omega}\right)^2 \tag{2.44}$$

Thus, across a bandpass $\Delta\omega$, the difference in the phase speed across the band differentially delays a periodic signal. This would normally not be an issue since the sources are not, in general very rapidly variable. But that is not the case for pulsars. For a pathlength *ds* the change in the arrival time is the same as a phase shift. Pulsars, magnetized rotating neutron stars with periods of from milliseconds to several seconds, are especially well suited to measure this. They have strong centimeter radio pulses and their intrinsic width is a fraction of the rotation period. The delay time can be determined using digital de-dispersing through the *dispersion measure*, DM:

$$DM = \frac{\Delta\omega}{c}\int nds \sim \int \frac{\omega_p^2}{\omega^3} ds \tag{2.45}$$

that is proportional to the electron column density along the line of sight. Fluctuations in n_e therefore introduce a variation in this measure and also are a driver of scintillation of Galactic and extragalactic radio sources (leading to finite angular diameters). Models based on the combined effects are discussed by Lazio and Cordes (2002) and Cordes and Lazio (2003). The propagation of polarized radio signals is also disturbed by the intervening magnetic field but, differently than the electron density, it is not isotropic and has several features that strongly differ. Across the same bandpass, right- or left-handed polarized continuum have different indices of refraction. The intervening electrons, tied to magnetic field lines, have a definite helicity depending on the orientation of the field. Calling the background field $\mathbf{B}_0$, oriented along the line of sight, the electron Larmor frequency (cyclotron frequency) is $\omega_L = eB_0/m_e c$. The *rotation measure*, measured in rad m^{-2} is the angle through which the plane of polarization is rotated,

$$RM = \frac{C}{\omega^2}\int \mathbf{B}\cdot\hat{k}n_e ds \tag{2.46}$$

which defines the *Faraday depth*

$$\phi(s_0) = \frac{e^3}{2\pi m_e^2 c^4}\int_{s_0}^{0} n_e(s)\mathbf{B}(s)\cdot\hat{k}ds \tag{2.47}$$

(Opermann et al. 2012), where the viewing direction is along $\hat{k}$. The result is the mean line of sight projected magnetic field and that is the core problem. This is *not* the field strength averaged over the electron column density. Instead, it is the *projected* field that can produce either sign of the rotation angle, depending on the relative orientation of the field lines toward the observer. Therefore, in a turbulent, or merely randomly oriented, field, the line of sight component may average to zero despite the energy density in the field possibly being large. It does not matter how closely spaced the frequencies are within the bandpass chosen for the observation. The only way out is to choose a scale for multiple lines of sight that is considerably larger than a single beam to capture some of the large scale structure. With the exception of a few high latitude clouds, the field in the diffuse medium can only be derived on a rather large scale, of order tens of parsecs or larger, because of the sparse sampling afforded by radio sources. This has significantly improved in recent years (see Opermann et al. 2012; Planck Collaboration, Plank 2015 results, paper XXI)), but it remains limited to line of sight only and requires substantial modeling efforts to disentangle orientation from field strength (e.g., Biermann and Kronberg 2004).

References

Abgrall et al. 1993, J,. Mol. Spec., 157, 512
Adams, W.S. 1941, ApJ, 93, 11
Athay, R.G. 1972, *Research in Radiative Transfer at NCAR*, Reidel Publishing Co.
Bailey, M., van Loon, J.Th., Sarre, P.J., adn Beckman, J.E. 2015, MNRAS, 454, 4013
Biermann, P. and Kronberg, P. P. 2004, JKAS, 37, 527
Campbell, E.E.B., Holz, M., Gerlich, D., and Maier, J.P. 2015, *Nature*, 523, 322
Cardelli, J.A, Clayton, G.C., and Mathis, J.S. 1989, ApJ, 345, 245
Chandrasekhar, S. 1950, *Radiative Transfer*, Oxford University Press
Cordes, J. and Lazio, J. 2003, http://arxiv.org/abs/astro-ph/0301598
Cowley, C.R. 1970, *The Theory of Stellar Spectra*, Gordon and Breach
Crutcher, R. 2012, ARAA, 50, 29
Crutcher, R. 2014, 69^{th} International Symposium on Molecular Spectroscopy, June 16–20, at the University of Illinois at Urbana-Champaign, Talk TF15
de Vries, H.W., Heithausen, A., and Thaddeus, P. 1987, ApJ, 319, 723
Dickey, J.M. and Lockman, F.J. 1990, ARAA, 28, 215
Draine, B.T. 2003, ARAA, 41, 241
Draine, B.T. 2011, *Physics of the Interstellar and Intergalactic Medium*, Princeton University Press
Ewen, H.L. and Purcell, E.M. 1951, *Nature*, 168, 350
Field, G.B. and Hitchcock, J.L. 1966, PRL, 16, 817
Field, G.B. and Hitchcock, J.L. 1966, ApJ, 146, 1
Fitzpatrick, E.L. and Massa, D. 1990, ApJS, 72, 163
Fitzpatrick, E.L. and Massa, D. 2007, ApJ, 663, 320
Fixsen, D.J. 2009, ApJ, 707, 916
Gatuzz, E., García, J. A., Timothy R. Kallman, T. R. and Mendoza, C. 2016, A&A, 588, A111
Gir, B.-Y., Blitz, L., and Magnani, L. 1994, ApJ, 434, 162
Goldreich, P. and Kylafis, N.D. 1981, ApJ, 243, 75
Griem, H.R. 1964, *Plasma Spectroscopy*, McGraw-Hill, New York

Griem, H.R. 1997, *Principles of Plasma Spectroscopy*, Cambridge Unversity Press
Güver, T. and Özel, F. 2009, MNRAS, 400, 2050
Harrison, S., Faure, A., and Tennyson, J. 2013, MNRAS, 435, 3541
Hartmann, J. 1904, ApJ, 19, 268
Hartmann, D. and Burton, W.B. 1997, *Atlas of Galactic Neutral Hydrogen*, Cambridge University Press
Herbig, G. 1975, ApJ, 196, 129
Hoyle, F. 1950, Observatory, 70, 194
Hubeny, I. and Mihalas, D. 2014, *Theory of Stellar Atmospheres*, Princeton University Press
Jackson, J.D. 1999 *Classical Electrodynamics*, 3rd ed., John Wiley & Sons
Jenkins, E. 1996, ApJ, 471, 292
Jenkins, E.B. 2009, ApJ, 700, 1299
Kalberla, P.M.W. et al. 2005, A&A, 440, 775
Kaplan, S.A. and Pikel'ner, S.B. 1970, *The Interstellar Medium*, Harvard University Press
Lazio, J. and Cordes, J. 2002, http://arxiv.org/abs/astro-ph/0207156v3
Li, D. and Goldsmith, P.F. 2003, ApJ, 585, 823
Lodders, K. 2003, ApJ, 591, 1220
McKellar, A. 1940, PASP, 52, 187
McKellar, A. 1941, PDAO, 7, 251
Merrill, P.W. 1938, *The Nature of Variable Stars*, The Macmillan company
Muller, C.A. and Oort, J.H. 1951, *Nature*, 168, 357
Moriarty-Schieven, G.H. and Wannier, P.G. 1997, ApJ, 475, 642
Opermann, N., et al. 2012, A&A, 542, A93
Osterbrock, D.E. and Ferland, G.J. 2006, *Astrophysics of Gaseous Nebulae and Active Galactic Nuclei*, 2nd ed., University Science Books
Palazzi, E, et al. 1990, ApJ, 357, 14
Peek, J.E.G., et al. 2011, ApJS, 194, 20
Planck Collaboration XXI, Plank 2015 results, A&A, 5765, 106
Ritchey, A.M., Federman, S.R., and Lambert, D.L. 2011, ApJ, 728, 36
Rybicki, G.B. and Lightman, A.P. 1979, *Radiative Processes in Astrophysics*, John Wiley & Sons, Inc.
Savage, B.D., Bohlin, R.C., Drake, J.F., and Budich, W. 1977, ApJ, 216, 291
Savage, B.D. and Sembach, K.R. 1996, ARAA, 34, 297
Sellgren, K. 1983, AJ, 88, 985
Shore, S.N., Magnani, L., LaRosa, T.N., and McCarthy, M.N. 2003, ApJ, 593, 413
Snow, T.P., Rachford, B.L., and Figovski, L. 2002, ApJ, 573, 662
Spitzer, L. Jr. 1978, *Physical Processes in the Interstellar Medium*, John Wiley & Sons, Inc.
Stecher, T.P. and Williams, D.A. 1966, ApJ, 146, 88
Thaddeus, P. and Clauser, J.F. 1966, PRL, 16, 819
Tielens, A.G.G.M. 2008, ARAA, 46, 289
Tielens, A.G.G.M. 2014, *The Diffuse Interstellar Bands, Proceedings of the International Astronomical Union, IAU Symposium*, Volume 297, 399
Wilson, O.C. and Merrill, P.W. 1937, ApJ, 86, 44

http://www.springer.com/978-3-662-54348-1

A Dirty Window
Diffuse and Translucent Molecular Gas in the Interstellar Medium
Magnani, L.; Shore, S.N.
2017, XIX, 306 p. 76 illus., 28 illus. in color., Hardcover
ISBN: 978-3-662-54348-1